

# A Deep RL Approach on Task Placement and Scaling of Edge Resources for Cellular Vehicle-to-Network Service Provisioning

Cyril Shih-Huan Hsu, Jorge Martín-Pérez, Danny De Vleeschauwer,  
Luca Valcarengi, Xi Li, Chrysa Papagianni

**Abstract**—Cellular Vehicle-to-Everything (C-V2X) is currently at the forefront of the digital transformation of our society. By enabling vehicles to communicate with each other and with the traffic environment using cellular networks, we redefine transportation, improving road safety and transportation services, increasing the efficiency of vehicular traffic flows, and reducing environmental impact. To effectively facilitate the provisioning of Cellular Vehicular-to-Network (C-V2N) services, we tackle the interdependent problems of service task placement and scaling of edge resources. Specifically, we formulate the joint problem and prove that it is not computationally tractable. To address its complexity we propose Deep Hybrid Policy Gradient (DHPG), a new Deep Reinforcement Learning (DRL) approach that operates in hybrid action spaces, enabling holistic decision-making and enhancing overall performance. We evaluated the performance of DHPG using simulations with a real-world C-V2N traffic dataset, comparing it to several state-of-the-art (SoA) solutions. DHPG outperforms these solutions, guaranteeing the 99<sup>th</sup> percentile of C-V2N service delay target, while simultaneously optimizing the utilization of computing resources. Finally, time complexity analysis is conducted to verify that the proposed approach can support real-time C-V2N services.

**Index Terms**—cellular vehicle to network, task placement, edge resource scaling, deep reinforcement learning.

## I. INTRODUCTION

**T**he term “Cellular Vehicle-to-Everything” (C-V2X) refers to the communication system that utilizes Long-Term Evolution (LTE) and/or 5G cellular technologies to facilitate seamless communication among vehicles, infrastructure, pedestrians, and other road users, establishing a comprehensive intelligent transportation ecosystem. The “Everything” in C-V2X refers to vehicles (V2V), infrastructure (V2I), pedestrians (V2P), and the network (V2N) [1], [2]. C-V2X technology’s primary objective is to improve road safety, enhance transportation system efficiency, and elevate the overall driving

experience [3]. Standardization of C-V2X technology is conducted by organizations like the 3rd Generation Partnership Project [4] and corporate coalitions like the 5G Automotive Association (5GAA)<sup>1</sup>.

In particular, C-V2N communication allows the C-V2X device to utilize the cellular network connection through the logical interface between the UE and the base station (Uu interface), to support applications/services such as advanced driver-assistance and collision avoidance; tele-operated driving; platooning (on highways); infotainment (e.g., video streaming to passengers in the vehicles); etc. Such applications, also require process-intensive and low-latency, reliable computing capabilities that the current vehicles with limited computation resources cannot meet. In this sense, offloading of tasks in a vehicular environment, that is transferring a workload to resource-rich computing platforms on external servers, is a viable solution for resource-constrained vehicles [5]. However, outsourcing to data centers can lead to increased delays, including transmission and processing delays due to CPU loads, as well as queuing delays from network congestion. In contrast, Edge Computing (EC) that provides computing resources and services at the edge of the network, closer to the devices and applications, is an effective approach to overcome delay challenges. Efficiently employing resources across the edge-to-cloud continuum for C-V2X applications, is considered a basic requirement for evolving 6G-V2X to provide more user-aware, scalable, and low-latency services for vehicles [6].

In this paper, we consider a C-V2N application supported by edge computing resources spanning multiple Points of Presence (PoPs) distributed throughout the metropolitan area of a city. We assume that application tasks per vehicle can be offloaded to any PoP which are interconnected throughout the city networks. In order to avoid degradation in the C-V2N application performance we need to address efficiently the resource allocation problem that consists of:

- 1) *Task Placement*: deciding where (i.e., in which PoP) to process the application tasks (e.g., decoding, sensor data processing, etc.) for each vehicle, given the availability of computing resources in each PoP;
- 2) *Scaling*: vertically scaling application resources at each PoP, to support offloaded tasks in a cost-efficient manner.

Cyril Shih-Huan Hsu and Chrysa Papagianni are with University of Amsterdam

E-mail: {s.h.hsu, c.papagianni}@uva.nl

Jorge Martín Pérez is with Departamento de Ingeniería de Sistemas Telemáticos, Universidad Politécnica de Madrid.

E-mail: jorge.martin.perez@upm.es

Danny de Vleeschauwer is with Nokia Bell Labs

E-mail: danny.de\_vleeschauwer@nokia-bell-labs.com

Luca Valcarengi is with Scuola Superiore Sant’Anna

E-mail: luca.valcarengi@santannapisa.it

Xi Li is with NEC Laboratories Europe

E-mail: Xi.Li@neclab.eu

Manuscript sent in 2024

<sup>1</sup><https://5gaa.org/about-us/>

These decisions are interdependent. On one hand the placement of application tasks determines the computing requirements per PoP, that drive scaling decisions. On the other hand scaling decisions define the maximum available computing resources per PoP that is further used as input for deciding on task placement. Moreover, the C-V2N application load fluctuates due to the dynamic flow of vehicle traffic. This leads to computing requirements per PoP that vary over time. Furthermore, task placement decisions may not always depend on a vehicle’s proximity to a PoPs. As long as delay requirements are met, it may be more cost-effective to process a vehicle’s tasks at a PoP outside its immediate vicinity—particularly in cases where such a decision would lead to resource scaling.

In summary, the key challenges in C-V2N scenarios include: (i) the real-time processing requirements of C-V2N applications, often within milliseconds; (ii) the dynamic nature of application traffic, which fluctuates over time; and (iii) the large-scale network problem involving multiple PoPs and a high volume of vehicles moving through metropolitan areas. These challenges demand scalable and compute-efficient solutions to solve the joint problems in a near-optimal and time-efficient manner. However, traditional centralized optimization approaches are not practical for addressing them. One reason is that the workload and resource dynamics of PoPs cannot be updated in a timely and synchronized manner, especially in city-wide scenarios where PoPs are widely dispersed. Additionally, decisions made centrally may not be communicated or enforced at each PoP in time, depending on the status of signaling channels. Lastly, traditional optimization methods often struggle with large-scale problems due to the substantial computational efforts required. Therefore, in this work we propose to leverage advanced AI methods to explore data driven solutions to address the above challenges.

### A. Contributions

The main contributions of this work are summarized below:

- 1) We first formulate the task placement and resource scaling decisions as a joint optimization problem, considering the latency constraints of the C-V2N application and cost-efficiency, in terms of the employed computing resources. The problem is initially formulated with the assumption of perfect knowledge of all future vehicle arrivals. We prove that the problem is  $\mathcal{NP}$ -hard and that the solution fosters meeting the 99<sup>th</sup> percentile delay requirement.
- 2) To account for the stochastic nature of traffic loads and the availability of physical resources, we formulate the joint problem as a Markov Decision Process (MDP), assuming no prior information about future vehicle arrivals. We introduce a new Deep Reinforcement Learning (DRL) approach called Deep Hybrid Policy Gradient (DHPG), to support a hybrid action space that encompasses both discrete and continuous actions, accommodating the different placement and scaling decisions. The proposed approach involves (i) a state encoder that maps the high-dimensional joint state into a compact latent space, providing a noise-reduced representation with rich information; (ii) this joint representation is shared across specialized action heads, allowing each of them to make more

holistic and well-informed decisions independently; (iii) we introduce the probability-as-action (PAA) approach, which allows for a differentiable representation of the hybrid action space, enabling actions from different actors to be optimized jointly with a single critic. This unified optimization results in faster convergence by ensuring more consistent gradient updates throughout the entire network.

- 3) We compare the proposed DHPG approach to different SoA methods, introduced in [7], [8] and [9]. We further use the “ideal” exact solution of the  $\mathcal{NP}$ -hard problem to derive optimality gaps for the selected approaches. To assess performance in realistic scenarios, we developed a simulator with real world traffic data. The simulation operates at the timescale of vehicle arrivals (in seconds) while capturing task arrivals at finer timescales (in milliseconds) by employing queuing model approximations for task processing delays. Running the simulation at the granularity of arriving vehicles allows us to investigate performance over extended time spans (hours or days) and examine the differences in performance between busy and off-peak hours.

The proposed DHPG effectively addresses aforementioned key challenges in C-V2N applications. First, its concise design allows for processing speeds in the sub-millisecond range, meeting the stringent real-time requirements of these applications in terms of 99-percentile delay guarantees. Second, by formulating and solving the problem as an MDP, DHPG inherently adapts to the dynamic nature of application traffic, allowing the system to respond to fluctuations over time. At last, the use of a joint latent space, which captures a compact representation of the global system state, along with the use of a hybrid action space, enables joint decision-making with reduced input dimensionality. The use of a single critic for different types of actions further simplifies training by avoiding the need for multiple critics, leading to more efficient learning and better scalability on a large scale. To the best of our knowledge, the proposed DHPG is the first end-to-end (E2E) DRL framework that directly considers the full joint task placement and scaling action space in a single step without relying on heuristics or approximations that may reduce the solution space, and is specifically designed to accommodate dynamic vehicle traffic changes in real-time. These features make DHPG a robust and scalable solution for the complexities of C-V2N environments.

The remainder of this paper is organized as follows. In Section II we provide a brief review of the related problems and the corresponding solutions. In Section III we describe the problem in mathematical terms and provide its formulations. Section IV details our proposed approach. Section V describes the simulation environment and the supported C-V2N application. We evaluate the proposed approaches in Section VI. Finally, Section VII further discusses the main findings of this paper and points out future research directions.

## II. RELATED WORK

In this section, we review the literature on resource scaling, task offloading, and the joint optimization problem.

**Resource Scaling.** Resource scaling is crucial in edge computing environments, particularly for services with highly variable traffic demands and sensitivity to latency. The challenge lies in dynamically adjusting the allocated computational resources to meet service demands while optimizing factors such as cost, energy efficiency, and service quality. Authors in [10] classify auto-scaling techniques for IoT-based cloud applications as either schedule-based or rule-based solutions. Specifically, they identify threshold-based policies, queuing theory, control theory, time-series analysis, and Reinforcement Learning (RL) as examples of rule-based approaches. Among these, threshold-based policies define specific upper or lower bounds for performance metrics, triggering scaling actions when these thresholds are crossed. In [11], authors use classification-based Machine Learning (ML) solutions to predict if scaling actions are necessary based on current network conditions. Moreover, authors in [12] propose an ML-based method that can assist in proactive auto-scaling by forecasting the number of VNF instances. Authors in [13] investigate the application of DRL in solving resource management for network slicing scenarios. Additionally, authors in [7] propose to vertically scale V2N services using a variant of Deep Deterministic Policy Gradient (DDPG) that captures the structure of the discrete action space to avoid the curse of dimensionality.

Forecasting traffic demands is also crucial, as it provides insights on the scaling operation. Related studies use classic time-series techniques such as Autoregressive Integrated Moving Average (ARIMA) or glstes [14], [15], Neural Network (NN) solutions based on Long Short Term Memory (LSTM) cells [16], [17], convolutional neural networks [18], or even Graph Neural Network (GNN)s [19]. While AI/ML approaches offer powerful capabilities, they typically require substantial amounts of data and computational resources, which may be a limiting factor in certain contexts. In contrast, traditional time-series forecasting techniques often demand fewer computational resources and lower energy consumption due to their reliance on simple analytical formulas. Studies such as [8], [9] have compared the trade-offs between traditional and AI/ML solutions for forecast-assisted scaling.

**Task Offloading/Placement.** Task offloading is a crucial aspect of edge computing, enabling resource-constrained devices to delegate computationally demanding tasks to more powerful edge nodes or cloud servers. The goal is to enhance the overall performance, reduce latency, and improve energy efficiency. The decision on whether or not to offload a task depends on various factors, including the computational requirements of the task, the available resources of the device and the edge nodes, and the latency of the network. The early approaches to task offloading [20]–[22], were primarily based on low complexity optimization algorithms, which can be simple and computationally efficient, but often led to suboptimal performance. To address this limitation, researchers have explored dynamic task offloading strategies that employ machine learning techniques [23], [24]. Several DRL-based task offloading frameworks have been proposed in the recent literature. The authors in [25] present the double deep Q-network (DDQN) approach for optimizing resource allocation in heterogeneous networks. Computation offloading in Mobile Edge Computing

(MEC) and Internet of Things (IoT) devices with DRL has been explored in several studies, including [26]–[31]. These frameworks typically employ deep NNs to represent the offloading policy, which learns to map task characteristics and network conditions to optimal offloading decisions. The frameworks differ in their choice of neural network architecture, reward function design, and training methodology.

**Joint Task Offloading/Placement and Resource Scaling.** The joint optimization of resource scaling and task offloading aims to address the limitations of treating these problems separately by considering their interdependencies, thereby enhancing overall system performance. The joint problem of task offloading and resource allocation at the edge, which involves a wider range of resources and resource management strategies, has been widely investigated in literature.

In [32], authors proposed an online joint offloading and resource allocation framework in an energy-constrained MEC network, explicitly considering the task delay, energy consumption and MEC long-term energy, using Lyapunov optimization. Authors in [33] proposed a computation offloading and resource allocation scheme. The problem is decoupled into two sub-problems for the offloading mode selection and the resource allocation, and solved by a distributed iterative algorithm. Problem decoupling is also used in [34], where the total energy consumption subject to the service latency requirement is minimized by jointly optimizing the task offloading ratio and resource allocation. In [35], authors addressed the placement and allocation problem in heterogeneous multi-server systems using an efficient approximation algorithm. Their approach focused on maximizing overall utility in static scenarios based on both synthetic and real-world utility functions.

Authors in [36], minimize the total execution latency and energy consumption, by jointly optimizing the task allocation decision and the CPU frequency of mobile devices, using a semi-definite relaxation-based approach. Authors in [37] employ Markov approximation to jointly optimize task assignment and CPU frequency scaling of mobile devices. Similarly, Authors in [38] proposed a DDPG-based framework to adjust the levels of both transmission power and local execution (CPU-cycle frequency) power. In [39], authors address the joint optimization of computation offloading and resource allocation in a dynamic MEC system, considering constraints like task completion time and energy consumption of mobile devices. Specifically, a DDPG-based method was proposed to optimize the offloading ratio, the computing power on mobile devices, and the uplink transmission power for offloading.

Recent works have started to explore this joint optimization in the context of V2X. Authors in [40] investigated the joint allocation of spectrum, computing, and storage resources in a MEC-based vehicle network using DDPG. The problem of joint offloading and resource allocation for vehicular edge computing with result feedback delay was studied in [41], where the task offloading decisions, the uplink bandwidth allocation and the computation resources allocation on the roadside unit are jointly optimized using an approximate algorithm. In [42], the authors presented a two-stage algorithm. The initial stage employs an optimization-based method to determine offloading decisions, followed by a multi-agent DDPG

approach to adjust transmission power for efficient resource scaling. A Twin Delayed DDPG (TD3)-based DRL approach was introduced in [43] to derive the optimal decision for task offloading, computation load ratio, and bandwidth allocation ratio. In [44] a game-theoretical approach is introduced for resource allocation and task offloading for vehicular edge networks, where the intra-server resource allocation and inter-server load-balanced task offloading are jointly optimized.

In this study, we assume that tasks are fully offloaded and we further expand the decision space by considering all available edge servers in the area as potential candidates for task placement, provided latency constraints are met. While this larger search space increases the complexity of the problem, it also creates opportunities to improve overall system performance. By dynamically distributing computational loads across multiple servers, we can reduce bottlenecks, optimize resource utilization, and minimize costs by avoiding unnecessary scaling actions and overprovisioning of resources.

To the best of our knowledge, the proposed DHPG is the first E2E DRL framework that has direct access to the full joint task placement and scaling action space in a single step without resorting to heuristics or approximations, while designed to handle dynamic vehicle traffic variations in real-time and in a large scale. Unlike existing approaches that often address task offloading/placement and resource scaling in a decoupled or sequential manner (e.g., [32]–[34], [42], [44]), rely on approximations (e.g., [35]–[37], [41]), and/or focus on the system’s short-term performance or static scenarios (e.g., [35]–[37], [41], [44]), DHPG captures the interdependencies between these tasks within a unified framework, and optimizes the long-term performance of dynamic systems. While step-wise/heuristic approaches may offer efficient solutions, they often implicitly reduce the search space by solving sub-problems in a pre-defined order (e.g., optimizing scaling before task placement) or introduce additional dependencies between decision variables through heuristic steps (e.g., using a greedy approach to find the placement strategy that minimizes latency based on the current scaling decision). In contrast, DHPG avoids these limitations by jointly optimizing both tasks. Furthermore, by using real-world traffic data and addressing stringent latency constraints, such as maintaining the 99<sup>th</sup> percentile of service delay within acceptable limits, the study goes beyond simply improving cost-efficiency to ensure reliable and high-quality service performance.

### III. SYSTEM MODEL AND PROBLEM FORMULATION

In this section we provide the system model and the associated problem formulation (i) as a combinatorial optimization problem, and (ii) as an MDP.

#### A. System Model

**Infrastructure.** We consider a set of  $P$  PoPs distributed throughout a city. Each PoP  $p \in \{1, \dots, P\}$  has a maximum processing capacity of  $C_p^{max}$ . Vehicle  $v \in \{1, \dots, V\}$  arrives at time instance  $t_v$  at the vicinity of a PoP that we denote as  $p_v$ . A Base Station (BS) (i.e., gNodeB) provides network connectivity to this vehicle  $v$  in the vicinity of the PoP  $p_v$ .

The application tasks stemming from the C-V2N application running on vehicle  $v$  are either processed locally at the PoP  $p_v$ , or redirected to be processed at another PoP  $p \neq p_v$ . The vehicle  $v$  leaves the vicinity of PoP  $p_v$  at time  $T_v > t_v$ . At that time, vehicle  $v$  either leaves the system altogether or enters the vicinity of another PoP.

**Application.** We consider a C-V2N application scenario, where each task is defined as a *basic unit of work to be executed towards the accomplishment of an application service* [45]. For example, in this study we employ a C-V2N application where each vehicle  $v$  produces a video sequence to be processed at the edge; each frame is decoded and analysed at some PoP  $p_v \in P$ , constituting the application task, as described in detail in Section V. We assume that every vehicle  $v$  sends  $\lambda$  tasks/s to its associated PoP during the interval  $[t_v, T_v]$ . We denote as  $d_{p,v}$  the processing delay experienced by tasks in PoP  $p_v$  right after the arrival of vehicle  $v$  at time  $t_v$ . As we focus on the performance impact of task offloading from the vehicle to edge computing resources, we define the task execution delay, which includes transmission and processing delay. To experience a good application quality, this task execution delay should be bounded by  $d_{tgt}$ .

**Task Placement.** When vehicle  $v$  enters the vicinity of PoP  $p_v$  at time  $t_v$ , a placement decision needs to be made for offloading the task(s) of the particular vehicle. The decision is captured in the decision variable  $p'_v$ ; the C-V2N tasks of that vehicle  $v$  will be processed at the PoP near the vehicle if  $p'_v = p_v$ , or at another PoP when  $p'_v \neq p_v$ . Note that the placement decision  $p'_v$  is made at time  $t_v$  and it remains valid until the vehicle  $v$  leaves the vicinity of PoP  $p_v$  at time  $T_v$ . Redirecting the tasks of vehicle  $v$  from PoP  $p_v$  to  $p'_v$ , introduces an additional transmission latency  $l_{p_v, p'_v}$ , but allows to tap into resources that could be potentially underutilised at PoP  $p'_v$ . The decision relies on information that PoP  $p_v$  exchanges with all other PoPs. In particular, it relies on the task processing delay that other PoPs experience when the

TABLE I: Notation Table

Symbol	Definition
$P$	number of PoPs
$V$	number of vehicles
$p$	PoP number
$v$	vehicle number
$t_v$	arrival instant of vehicle $v$
$T_v$	departure instant of vehicle $v$
$p_v$	PoP at which vehicle $v$ arrives ( $\in \{1, 2, \dots, P\}$ )
$p'_v$	PoP processing vehicle $v$ tasks
$N_p(t)$	number of vehicles processed at PoP $p$ at time $t$
$\lambda$	avg. task arrival rate generated by the Cellular Vehicle-to-Network (C-V2N) application
$C_{p,v}$	CPUs used by the C-V2N application at PoP $p$ right after $t_v$
$C_{p,v}^+$	CPU increase/decrease at PoP $p$ right after $t_v$
$C_p^{max}$	maximum processing capacity at PoP $p$
$\mu(C)$	service rate at PoP employing $C$ CPUs
$\rho_{p,v}$	load in PoP $p$ at time $t_v$
$\mathbb{E}[d_{p,v}]$	(average) processing delay in PoP $p$ at time $t_v$
$l_{p,p'}$	transmission delay between PoP $p$ and $p'$
$d_v$	total delay experienced by vehicle $v$
$d_{tgt}$	target delay
$R(\cdot)$	reward function to be optimized

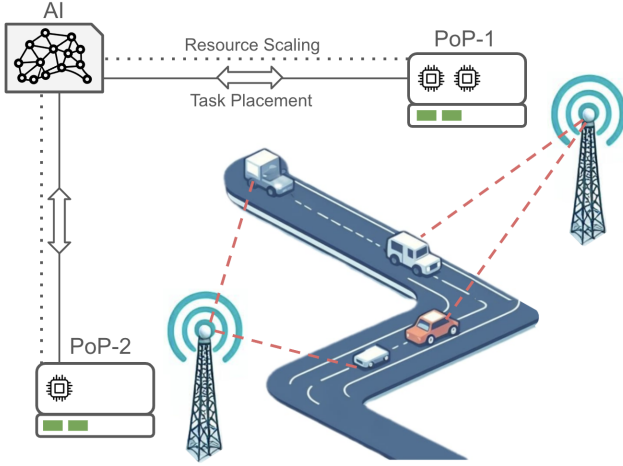


Fig. 1: System Overview

vehicle  $v$  arrived, which we denoted as  $d_{p,v}$ ,  $p \in P$ .

**Resource Scaling.** Scaling decisions determine the computing resources (number of CPUs)  $C_p(t)$  required in each PoP  $p \in P$  at regular instants  $t$ , with  $C_p(t) \leq C_p^{\max}$ ,  $\forall t$ . These instants  $t$  could be different from the vehicle arrival instants, e.g., they could occur periodically (e.g., every 5 minutes), but in this study we assume that they are aligned with vehicle arrival instants  $t_v$ , following the placement decisions. As a result, between consecutive *scaling* instants the decision variables  $C_p(t)$  remain constant, i.e.:

$$C_p(t) = C_p(t'), \quad \forall p, \forall t, t' \in [t_v, t_{v+1}) \quad (1)$$

Consequently, from now on we will use  $C_{p,v}$  to denote  $C_p(t_v)$ . Remark that in the set of all possible *scaling* decisions, the “no *scaling*” option is also included.

**Task Processing Delay.** The average task processing delay  $\mathbb{E}[d_{p,v}]$  in PoP  $p$  at time  $t_v$  can be estimated using a queuing model, given the task arrival and service processes. As each vehicle  $v$  sends  $\lambda$  tasks/sec to its associated PoP during the interval  $[t_v, T_v]$ , the task arrival process has an arrival rate  $\lambda N_{p,v}$ , where  $N_{p,v}$  denotes the number of vehicles assigned to  $p$  at  $t_v$  as follows:

$$N_{p,v} = \sum_{v' \in V: p'_{v'}=p} \mathbb{1}_{[t_v, T_{v'}]}(t_v) \quad (2)$$

$\mathbb{1}_A(x)$  is an indicator function, which is 1 when  $x \in A$ , and 0 otherwise. In line with [46]–[48], we model the task service process at each PoP with an M/G/1-PS queue, where PS stands for Processor Sharing, with a serving rate  $\mu(C_{p,v})$ . By modeling a PoP with an M/G/1-PS queue we assume that the arrival rate of vehicles’ tasks follow a Poisson distribution, and such assumption holds for sufficiently large task arrival rates according to the Palm-Khintchine theorem [49]. Regarding the service rate  $\mu(C_{p,v})$ , we do not make any assumption about its distribution. Similar to [46]–[48], we only consider that  $\mu(C_{p,v})$  increases as the number of CPUs  $C_{p,v}$  increases. Under the assumptions above, the average processing delay

$\mathbb{E}[d_{p,v}]$  at time  $t_v$  in PoP  $p$  is:

$$\mathbb{E}[d_{p,v}] = \begin{cases} \frac{1}{\mu(C_{p,v}) - \lambda N_{p,v}} & \text{if } \mu(C_{p,v}) > \lambda N_{p,v} \\ \infty & \text{otherwise} \end{cases} \quad (3)$$

**Task Total Delay.** In the average delay experienced by a task we consider both the transmission latency  $l_{p_v, p'_v}$  and processing delay  $d_{p'_v, v}$ . We define the experienced delay  $d_v$  as:

$$d_v = l_{p_v, p'_v} + \mathbb{E}[d_{p'_v, v}] \quad (4)$$

i.e.  $d_v$  is the sum of the worst transmission latency and average processing delay, which we compute using (3).

However, ensuring  $d_v \leq d_{tgt}$  does not guarantee that C-V2N tasks meet the delay requirement the 99% of the times. To that end, we define the  $\kappa$ -percentile of the experienced delay as:

$$d_v^\kappa = l_{p_v, p'_v}^\kappa + d_{p'_v, v}^\kappa \quad (5)$$

with  $l_{p_v, p'_v}^\kappa, d_{p'_v, v}^\kappa$  the  $\kappa$ -percentile of the transmission and processing latency, respectively. The expression for  $d_{p'_v, v}^\kappa$  depends on how processing times are distributed, i.e., it will vary depending on the C-V2N tasks. To remain as generic as possible, we resort to the well-known M/G/1-PS average delay (3) expression and bound the  $\kappa$ -percentile of the processing delay as  $d_{p'_v, v}^\kappa < K(\kappa) \cdot \mathbb{E}[d_{p'_v, v}]$ . Here,  $K(\kappa) \geq 1$  is a bound that depends on the percentile  $\kappa$ . With the aforementioned, we provide an upper bound denoted as  $\overline{d}_v^\kappa$ , i.e., an upper bound of the  $\kappa$ -percentile of the experienced task delay  $d_v^\kappa$ :

$$\overline{d}_v^\kappa = l_{p_v, p'_v} + K(\kappa) \cdot \mathbb{E}[d_{p'_v, v}] \quad (6)$$

Fig. 1 illustrates the placement of vehicles’ tasks to PoPs, and number of CPUs allocated to support their respective requirements at each PoP. Based on placement and scaling decisions made by the agent, vehicles offload application tasks (green blocks) to the associated PoP for processing, while the computational resources allocated per PoP are visualized by CPUs. In this example, PoP-1 is processing two tasks supported by two CPUs, while PoP-2 has two tasks supported by one CPU.

## B. Optimization Problem

In this section we assume that all vehicle arrival instants  $t_v$  and the PoPs  $p_v$  the vehicle arrive at are known. We formulate the task placement and scaling actions as an optimisation problem aiming to maximize an objective function  $R(\cdot)$  while taking the appropriate *task placement* and *scaling* decisions, i.e.: (i) which PoP  $p'_v$  has to process the C-V2N tasks produced by vehicle  $v$ ; and (ii) how many Central Processing Units (CPUs)  $C_{p,v}$  are required by PoP  $p$  to process the vehicles’ C-V2N tasks (just after the placement decision for vehicle  $v$  has been made until the arrival of the next vehicle).

**Problem 1** (Task placement and scaling).

$$\max_{C_{p,v}, p'_v} \sum_v \sum_p R(C_{p,v}, p'_v) \quad (7)$$

$$s.t.: C_{p,v} \leq C_p^{\max}, \quad \forall p, v \quad (8)$$

$$p'_v \in P, \quad \forall v \quad (9)$$

$$C_{p,v} \in \mathbb{N}, \quad \forall p, v \quad (10)$$

with  $R(C_{p,v}, p'_v)$  being the reward function that we obtain based on the *scaling* and *placement* decisions taken for vehicle  $v$  at the time  $t_v$  it arrives. Constraint (9) imposes that the C-V2N tasks of each vehicle are placed on a single PoP while (8) describes the processing capacity constraints (number of CPUs) at a PoP.

Since we aim to meet the delay constraint  $d_{tgt}$  of the C-V2N service, and minimize the number of CPUs that we employ at the PoPs; we resort to the following reward function:

$$R(C_{p,v}, p'_v) = \frac{d_v}{d_{tgt}} \cdot \exp\left(-\frac{1}{2} \left[\left(\frac{d_v}{d_{tgt}}\right)^2 - 1\right]\right) \quad (11)$$

with  $d_v$  dependent on both the *placement*  $p'_v$  and *scaling*  $C_{p,v}$  decisions, as they both impact transmission and processing delay based on formula (4).

Fig. 2 illustrates how the reward function (11) aims at meeting the target delay  $d_{tgt}$  without leading to over- or under-provisioning of computing resources (CPUs). Namely, over-provisioning resources  $C_{p,v}$  at the PoP will result in a delay lower than the target one  $d_{tgt}$  as we use more CPUs than necessary. Conversely, under-provisioning computing resources results in exceeding the target delay, decreasing the reward. The goal of the reward function is to push  $d_t$  toward  $d_{tgt}$ , while having its range bounded  $R(\cdot) \in [0, 1]$  that provides effective signals for training stability. Without a bounded range, rewards could go to plus/minus infinity when the latency is too small/large, which can hinder the learning of DRL agents by incurring extreme gradients during backpropagation. Moreover, the placement decision  $p'_v$  also impacts the reward, for processing the vehicle  $v$  tasks at a PoP  $p'_v \neq p_v$  results in a high transmission latency  $l_{p_v, p'_v}$ . As a result, the total delay may increase beyond the target  $d_{tgt}$  thus reducing the reward. Ideally, *placement* and *scaling* decisions should lead to a total delay as close as possible to the target  $d_{tgt}$ .

Notice that the reward function of (11) is nonlinear in the decision variables  $C_{p,v}$  and  $p'_v$  (via equation (4)). Taking logarithms on (11) would not suffice, as it would result to a processing delay term in the power of two. Moreover, when we substitute the processing delay with its average according to formula (3), we have a non-linear dependency with the number of CPUs  $C_{p,v}$  and the number of vehicles that a PoP processes. Additionally, the reward function (11) is not convex/concave in the decision variables, for the second derivative with respect to the delay with  $d = d_v/d_{tgt}$ , does not have the same sign for all  $d$ :

$$\frac{\partial^2}{\partial d^2} R(\cdot) = d(d^2 - 3) \exp\left(-\frac{d^2 - 1}{2}\right) \quad (12)$$

Therefore, we cannot drive the search of the optimal solution using the chain rule on the *task placement*  $p'_v$  and *scaling*  $C_{p,v}$  variables – note both variables determine the total delay  $d_v$  – as the search may be trapped in local optima. Achieving a global optimal solution for Problem 1 requires exhaustive search. However, in the following lemma we show that the problem is  $\mathcal{NP}$ -hard thus computationally intractable.

**Lemma 1.** *Problem 1 is  $\mathcal{NP}$ -hard.*

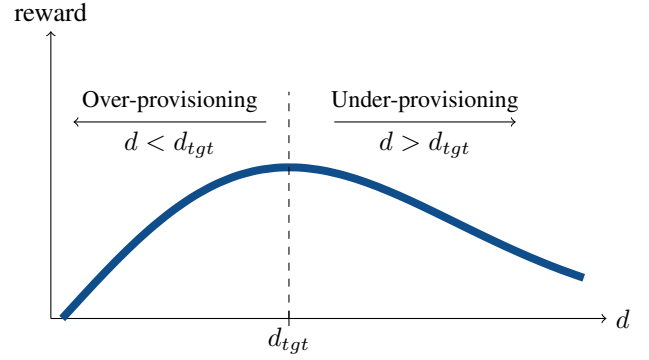


Fig. 2: Reward as function of the service delay  $d$ .

The proof is provided in Appendix A.

Despite the  $\mathcal{NP}$ -hardness of Problem 1 we use an “oracle” to get the optimal solution. The oracle knows in advance the arrival time  $\{t_1, t_2, \dots, t_V\}$  of every vehicle  $\{1, 2, \dots, V\}$ ; and plugs such values in the optimization problem to obtain the best *placement*  $p'_v$  and *scaling*  $C_{p,v}$  decisions. Due to the problem’s complexity, computing the oracle solution is only feasible for small instances of the problem. However we use it to derive optimality gaps to our proposed approach and other solutions we adapt from the state of the art.

Lastly, we replace the  $d_{tgt}$  term in the reward function by  $\frac{d_{tgt}}{K(\kappa)}$  to meet the  $\kappa$ -percentile of the delay.

**Lemma 2** ( $\kappa$ -percentile reward maximum). *Replacing  $d_{tgt}$  by  $\frac{d_{tgt}}{K(\kappa)}$  in (11) ensures that the maximum reward is achieved before  $d_v^\kappa$  reaches  $d_{tgt}$ .*

*Proof.* Replacing the  $d_{tgt}$  term in the  $\frac{d_v}{d_{tgt}}$  ratio from (11) results into the following inequality

$$\frac{\frac{d_v}{\frac{d_{tgt}}{K(\kappa)}}}{\frac{d_{tgt}}{K(\kappa)}} = \frac{K(\kappa)d_v}{d_{tgt}} > \frac{l_{p_v, p'_v} + K(\kappa)\mathbb{E}[d_{p'_v, v}]}{d_{tgt}} = \frac{\bar{d}_v^\kappa}{d_{tgt}} > \frac{d_v^\kappa}{d_{tgt}} \quad (13)$$

with the first inequality holding due to (4) and  $K(\kappa) \geq 1$ , and the latest equality given by the definition of  $\bar{d}_v^\kappa$  provided in (6). Consequently, if we replace the  $d_{tgt}$  term as specified in the Lemma statement, the maximum reward is achieved before the  $\kappa$ -percentile of the experienced delay reaches the target.  $\square$

Thanks to Lemma 2, we can select the  $d_{tgt}$  term, use the average processing delay from an M/G/1-PS queue (3), solve the optimization Problem 1, and ensure that the solution will foster meeting the  $\kappa$ -percentile delay requirement. Specifically, in Appendix B we show that setting the target delay to  $d_{tgt}/2$  and using the average delay formula of the M/G/1-PS, ensures meeting the  $d_{tgt}$  delay requirement 99% of the time.

### C. MDP Formulation

In reality, at the time placement and potentially scaling decisions are taken for vehicle  $v$ , the arrival times of future vehicles are not known. Therefore we reformulate Problem 1 (which assumes this knowledge) as an MDP. In particular, we define the state and action spaces, as well as the transition probabilities and reward of the considered MDP  $(\mathcal{S}, \mathcal{A}, \mathbb{P}, R)$ .

The state at the arrival time  $t_v$  of vehicle  $v$  is represented by the number of vehicles and CPUs at each PoP:

$$s_v = (p_v, N_{1,v}, C_{1,v}, \dots, N_{P,v}, C_{P,v}) \quad (14)$$

where  $p_v$  denotes the PoP at which vehicle  $v$  arrives, and we define  $s_{v,p} = (N_{p,v}, C_{p,v})$  as the state of PoP  $p$  upon the arrival of a vehicle  $v$ . Note that the state space is formally defined as  $\mathcal{S} = \mathbb{N}^{2P+1}$ . An action is then defined as:

$$a_v = (p'_v, C_{1,v}^+, \dots, C_{P,v}^+) \quad (15)$$

Therefore, the action space of our MDP is  $\mathcal{A} = \mathbb{N} \times \mathbb{Z}^P$ . The goal is to find a policy  $\pi : \mathcal{S} \mapsto \mathcal{A}$  that draws an action  $a_v \in \mathcal{A}$  when the system is in state  $s_v$ . This action for vehicle  $v$  consists of deciding in which PoP its C-V2N tasks will be processed  $p'_v$ , and determining the number of CPUs to scale to at each PoP  $C_{1,v}^+, \dots, C_{P,v}^+$ . For example  $C_{p,v}^+ = 1$  means that CPU at PoP  $p$  is scaled up by one, while vehicle  $v$  is placed to PoP  $p'_v$ . Negative values are associated with scaling down the number of CPUs.

The transition probabilities  $\mathbb{P}(s_{v+1}|s_v, a_v)$  express how likely it is to end up in a new state  $s_{v+1}$  based on the action  $a_v$  taken in the prior state  $s_v$ . In this context they depend upon the arrival process of the vehicles and their lingering time in the vicinity of each respective PoP. Note that the scaling decisions  $C_{p,v}^+$  within the action described by formula (15) determine the number of CPUs in the future state, namely  $C_{p,v+1} = \max\{0, C_{p,v} + C_{p,v}^+\}$ .

The last element to define in the MDP tuple is the reward function  $R(s_{v,p}, a_v)$ . As a reward function we employ the objective function used in the optimization Problem 1, i.e.,  $R(C_{p,v}, p'_v)$ .

Given the definition of the state space, action space, transition probabilities, and the reward function; we formulate the MDP.

**Problem 2** (Task placement and scaling). *Given the  $(\mathcal{S}, \mathcal{A}, \mathbb{P}, R)$  tuple, find a policy  $\pi$  that maximizes*

$$\mathbb{E}_{a_v \sim \pi, \mathbb{P}(s_v, a_v)} \frac{1}{P} \sum_v \gamma^v \sum_p R(s_{v,p}, a_v) \quad (16)$$

with the discount factor  $\gamma \in [0, 1]$ .

The goal of the MDP is to maximize the expected discounted reward, averaging over the reward obtained at each PoP over time. However, we do not make any assumption of how vehicles arrive to different roads where PoPs are located, nor the volume of road traffic over the day. Making such assumptions becomes hard when it comes to model unpredictable events as accidents, traffic jams, etc. Rather, we resort to a model-free approach to solve Problem 2.

#### IV. PROPOSED METHOD

To solve Problem 2 we need to jointly optimize placement and scaling decision variables, that are both discrete in nature. In our previous work [7], the resource scaling problem is tackled in a continuous fashion using the DDPG variant, to address the scalability problem inherent to the high-dimensional discrete action space. Specifically, we have

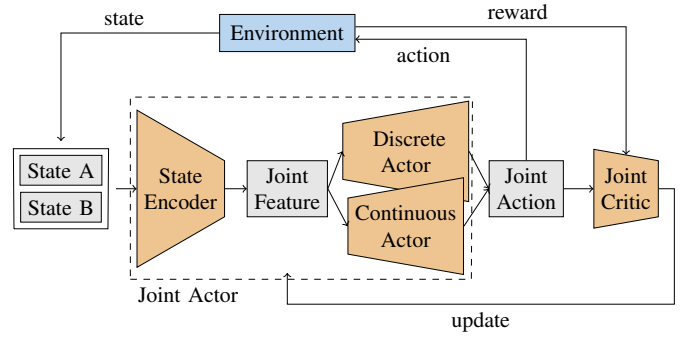


Fig. 3: Framework of DHPG. The states collected from the environment are first concatenated and sent to the state encoder to extract the joint feature. The feature is then fed to different actors to generate corresponding actions which are concatenated into a joint action. Finally the joint action is returned to the (i) environment and (ii) joint critic, along with the reward for learning. The details of the use of replay buffer and target networks are omitted for simplicity.

deliberately employed a continuous action space for scaling decisions, to enhance robustness against increasing dimensionality. On the other hand, handling the placement problem is trivial using discrete DRL algorithms like DQN [50], as it is a discrete decision-making process with a low-dimension action space. In this work, we extend this approach by combining continuous scaling decisions with discrete placement actions, resulting in a hybrid action space. However, jointly optimizing discrete and continuous decision variables under a single DRL framework is challenging. The main reason is because discrete and continuous actions often require different policy representations. For discrete actions, a tabular or probability distribution representation is common, while for continuous actions, a Gaussian distribution or other parametric function is typically used. Reconciling these different representations can be difficult. Furthermore, defining a reward decomposition which transforms the reward signal to effectively guide both discrete and continuous action selection is a non-trivial task. There have been a number of attempts to address this challenge, but there is no single, widely accepted solution. Some approaches involve discretizing the continuous action space, which can lead to loss of information. Others involve using separate learned models for the discrete and continuous actions, which can make the learning process more complex [51].

To this end, we propose Deep Hybrid Policy Gradient (DHPG), which operates inherently in hybrid action spaces. DHPG follows the learning framework of DDPG [52], but with the following novel components: (i) joint state encoder  $\mu_e$  which learns to extract compact and informative representations across various state spaces; (ii) specialized action heads ( $\mu_p, \mu_C$ ) that predict actions in different but correlated action spaces; and (iii) a new technique termed as probability-As-Action, which relaxes discrete actions into continuous representations, and thus allows E2E efficient learning under a unified framework. Fig. 3 illustrates the proposed framework. **Joint state encoder.** Traditional policy networks in DRL typically take a single state representation as input and output

a probability distribution over a set of actions. This approach has been successful in a variety of tasks, but it can be limited in its ability to capture the complex interactions between multiple state components, particularly in tasks with hierarchical or heterogeneous structures. The joint state encoder  $\mu_e$  takes a concatenated state representation  $s_v$ , which is a vector of state information from multiple components of the environment, as input. It then applies a series of neural network layers to extract a joint feature representation  $z_v = \mu_e(s_v | \theta^\mu)$  that captures the essential information about the state. Note that we adopt one-hot encoding for discrete states.

**Specialized action heads.** The joint feature representation is then passed to multiple dedicated actors, each responsible for generating actions for a specific component of the environment. In the case of Problem 2, the dedicated actors  $\mu_p, \mu_C$  take the placement and scaling decisions, respectively. These actors are also neural network models that take the joint feature representation  $z_v$  as input, and output: (i) a probability distribution representing the chances of placing a task to a specific PoP  $\mu_p(z_v | \theta^\mu) \in [0, 1]^P$ ; and (ii) real values over the corresponding continuous action space to decide the number of CPUs at each PoP  $\mu_s(z_v | \theta^\mu) \in \mathbb{R}^P$ . It is worth mentioning that the last layer of the discrete actor  $\mu_p$  is a softmax layer  $\sigma : \mathbb{R}^P \rightarrow [0, 1]^P$ , thus  $\mu_p(z_v | \theta^\mu) \in [0, 1]^P$ . The actions generated by the actors are concatenated into a joint action vector  $\hat{a}_v = [\mu_p(z_v | \theta^\mu), \mu_s(z_v | \theta^\mu)]$ . The joint action  $\hat{a}_v$  is passed to the joint critic which estimates the expected cumulative reward given the joint action and state.

**Probability-as-action.** The traditional approach handling discrete action spaces relies on sampling an action from a probability distribution, while continuous action spaces involve generating a real-valued action from a parametric function. This difference leads to incompatible approaches in optimization. To address these limitations, we propose a novel approach called probability-as-action (PAA), which takes the softmax-normalized vector directly as the action, rather than using a sampled action. This continuous relaxation of the discrete action allows for more nuanced policy representation and seamless integration with continuous action space algorithms. In PAA, the discrete actor produces a softmax-normalized vector  $\mu_p(z_v | \theta^\mu) \in [0, 1]^P$  representing the likelihood of each discrete action – e.g. the likelihood of placing the vehicle task at PoP 1, ..., P. This vector is directly used as the action representation passed to the critic. However, the actual action  $a_v$  sent to the environment is randomly selected according to the softmax-normalized vector. Hence, the same joint action  $\hat{a}_v$  may result in different actual actions  $a_v \neq a'_v$  during the training stage. Finally, since the reward is no longer in response to a specific sampled action but a probability distribution, the discrete actor  $\mu_p$  ends up learning to generate a probability distribution that leads to higher expected cumulative rewards.

Overall, the DHPG agent comprises discrete and continuous action heads  $\mu_p, \mu_C$  taking the placement and scaling decisions jointly. In the following we explain how the actual action  $a_v = (p'_v, C_{1,v}^+, \dots, C_{P,v}^+)$  is taken. During the training stage, the placement decision is chosen using a random sampling function  $X : [0, 1]^P \rightarrow \mathbb{N} \cap [1, P]$  over the softmax-normalized

---

**Algorithm 1** Learning of DHPG

---

- 1: Initialize joint actor  $\mu$  with parameters  $\theta^\mu$
  - 2: Initialize joint critic  $Q$  with parameters  $\theta^Q$
  - 3: Initialize target network  $\mu' \leftarrow \mu$  and  $Q' \leftarrow Q$
  - 4: Initialize replay buffer  $B$
  - 5: **for**  $episode = 1, E$  **do**
  - 6:   Receive initial state  $s_1$
  - 7:   **for**  $v = 1, V$  **do**
  - 8:     Extract joint latent representation  $z_v = \mu_e(s_v | \theta^\mu)$
  - 9:     Obtain placement probability  $y_p = \mu_p(z_v | \theta^\mu)$
  - 10:     Obtain scaling action  $y_C = \mu_C(z_v | \theta^\mu)$
  - 11:     Obtain joint action  $\hat{a}_v = [\sigma(y_p), y_C]$
  - 12:     Obtain executable actions:
  - 13:        $p'_v = X(\sigma(y_p))$
  - 14:        $(C_{1,v}^+, \dots, C_{P,v}^+) = \text{DOD}(y_C)$
  - 15:     Execute actions  $p'_v$  and  $(C_{1,v}^+, \dots, C_{P,v}^+)$
  - 16:     Observe reward  $r_v$  and next state  $s_{v+1}$
  - 17:     Store transition  $(s_v, \hat{a}_v, r_v, s_{v+1})$  in  $B$
  - 18:     Sample a random batch  $b$  of transitions in  $B$
  - 19:     Set  $y_v = r_v + \gamma Q'(s_{v+1}, \mu'(s_{v+1}))$ ,  $v \in b$
  - 20:     Update Critic using Bellman error:
  - 21:       
$$\delta \theta^Q = \frac{1}{|b|} \sum_{v \in b} \nabla_{\theta^Q} [y_v - Q(s_v, a_v)]^2$$
  - 22:     Update Actor using policy gradient:
  - 23:       
$$\delta \theta^\mu = -\frac{1}{|b|} \sum_{v \in b} \nabla_a Q(s_v, a) \nabla_{\theta^\mu} \mu(s_v)$$
  - 24:     Update target networks:
  - 25:        $\theta^{Q'} \leftarrow \tau \theta^Q + (1 - \tau) \theta^Q$
  - 26:        $\theta^{\mu'} \leftarrow \tau \theta^\mu + (1 - \tau) \theta^\mu$
  - 27:   **end for**
  - 28: **end for**
- 

vector – i.e.  $p'_v = X(\mu_p(z_v | \theta^\mu))$ . In the testing stage, the placement decision is taken based on the PoP reporting the highest likelihood – i.e.  $p'_v = \text{argmax}\{\mu_p(z_v | \theta^\mu)\}$ . The scaling decisions are produced after applying Deterministic Ordered Discretization (DOD) [7] for the output of the continuous action head, that is, the CPU scaling is obtained as  $(C_{1,v}^+, \dots, C_{P,v}^+) = \text{DOD}(\mu_C(z_v | \theta^\mu))$ . Note, however, that the training stage uses the continuous output (prior to the DOD) to feed the critic network. Algorithm 1 describes the DHPG learning procedure.

Lastly, it is worth mentioning that our solution DHPG comprises an end-to-end joint DRL approach that determines the placement decision  $p'_v$ , and a scaling vector  $(C_{1,v}^+, \dots, C_{P,v}^+)$  that specifies the CPU increment at each PoP based on the observed state  $s_v = (p_v, N_{1,v}, C_{1,v}, \dots, N_{P,v}, C_{P,v})$  across all PoPs. Note that DHPG differs from the decentralized Deep Deterministic Policy Gradient (DDPG) approach in [7], where a dedicated DDPG agent is in charge of scaling decisions at each PoP. Fig. 4 highlights the difference between the proposed DHPG solution, which utilizes global state information aggregated at each agent/PoP running the DHPG approach,

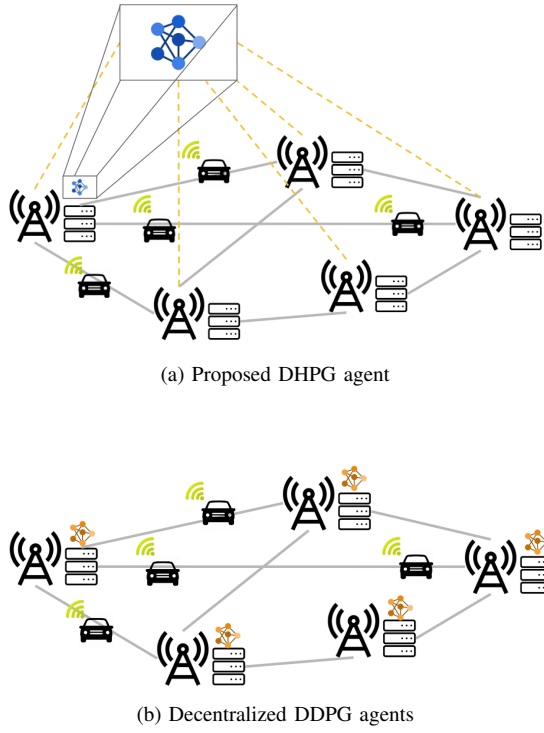


Fig. 4: The proposed DHPG agent vs. decentralized DDPG agents [7] for C-V2N service provisioning.

versus the purely decentralized DDPG scaling agent from [7] coupled with greedy-based placement agent. In Section VI we compare the performance of both approaches.

## V. V2N APPLICATION SERVICE SIMULATION

Following, we describe the simulation environment that we implemented to evaluate the performance of our approach, and describe the dataset used to drive the simulations.

### A. Simulation Environment

The simulation environment [53] implements the State–Action–Reward–State–Action (SARSA) [54] logic inherent to a MDP, i.e., it implements the functions required to perform actions  $a_v$ , to monitor the state  $s_v$ , and to report the rewards  $R(s_v, a_v)$  as the simulation progress. It is implemented in Python and consists of two main classes: (i) a class simulating the operations within the MEC node at each PoP, named *PoP queue*; and (ii) a class simulating and monitoring the metro environment, named *environment*. In the following, we explain in detail the classes of the simulation environment and their interactions – see Algorithm 2.

**PoP queue class.** The *PoP queue* class simulates the operations at PoP  $p$  level. Upon the arrival of vehicles  $v \in V$  it keeps track of the number of active CPUs  $C_{p,v}$ , how many vehicles  $N_{p,v}$  are attended by the PoP, what is its current load  $\rho_{p,v}$ , and what is the resulting processing latency  $d_{p,v}$ . The *PoP queue* class derives the processing delay and load as follows:

- *Processing delay*: to compute  $d_{p,v}$  using formula (3), we have to obtain the processing rate of the PoP  $\mu(C_{p,v})$ .

TABLE II: Time to decode  $\tau_d$  [55] and analyze  $\tau_a$  [56] a frame (f) using H.265/HEVC streams [57], and  $C_p$  Intel Xeon CPUs. Both contributions yield the Vehicle-to-Network (V2N) frame processing rate  $\mu$ .

	$C_p = 1$	$C_p = 2$	$C_p = 3$	$C_p = 4$	$C_p = 5$
$\tau_d$	8.47 ms/f	4.41 ms/f	3.05 ms/f	2.37 ms/f	2.03 ms/f
$\tau_a$	37 ms/f	18.50 ms/f	12.33 ms/f	9.25 ms/f	7.40 ms/f
$\mu$	0.02 f/ms	0.04 f/ms	0.06 f/ms	0.09 f/ms	0.11 f/ms

### Algorithm 2 Simulation Environment

- 1: Initialize environment env
- 2: Initialize total reward  $r_t \leftarrow 0$
- 3:  $s_v, r_v, \text{stop} \leftarrow \text{env.step}()$
- 4: **while** not stop **do**
- 5:      $r_t \leftarrow r_t + r_v$
- 6:      $p'_v, a_v \leftarrow \text{DHPG}(s_v)$
- 7:      $s_v, r_v, \text{stop} \leftarrow \text{env.step}(p'_v, a_v)$
- 8: **end while**
- 9: **return**  $r_t$

This rate is derived considering the video decoding  $\tau_d$  and analysis contributions  $\tau_a$ . Specifically, we estimate the processing rate as  $\mu(C_{p,v}) = \frac{1}{\tau_d(C_{p,v}) + \tau_a(C_{p,v})}$ , with  $\tau_d$  set using the empirical evidence presented in [55], and  $\tau_a$  as presented in [56]. Table II summarizes the processing rates  $\mu$ , as well as the decoding and analysis contributions.

- *Load*: the current load per PoP is estimated using the number of served vehicles  $N_{p,v}$  and active CPUs  $C_{p,v}$ . In particular, the load is set to  $\rho_{p,v} = \lambda N_{p,v} / \mu(C_{p,v})$ , where  $\lambda = 29.5$  fps per H.265/HEVC stream (ETSI [57] V2N services).

**Environment class.** The *environment* class keeps track of the set  $P$  of *PoP queue class instances* and interacts with them to monitor the system state  $s_v$ , take actions  $a_v$ , and report the obtained rewards  $R(s_v, a_v)$ . All such interactions are driven by the instants at which vehicles arrive  $\{t_1, t_2, \dots, t_V\}$  according to the used dataset – see Section V-B. In the following we enumerate the *environment* interactions:

- i) Upon the arrival of a vehicle  $t_v$ , the *environment* class iterates over *PoP classes* and removes those vehicles  $v'$  that already left each PoP  $p$ , i.e., those with  $T_{v'} < t_v$ .
- ii) The *environment* reports the system state  $s_v$  in (14) by retrieving from each *PoP queue* the number of vehicles it is serving  $N_{p,v}$ , and the number of active CPUs  $C_{p,v}$ .
- iii) The DHPG agent takes the state  $s_v$  across all PoPs and returns an action  $a_v$  that contains the placement  $p'_v$  and scaling decisions  $C_{p,v}^+, \forall p \in P$  to the *environment* class.
- iv) The *environment* class assigns the vehicle  $v$  and places its corresponding tasks to the *PoP queue*  $p'_v$  and sets its departure time as  $T_v = t_v + 30k$ , with  $k \sim \text{Exp}(\Lambda)$  drawn from an exponential distribution with rate  $\Lambda = 1$ , i.e., on average vehicles linger for 30 sec in the road. Then, the *environment* iterates over each *PoP queue* to scale its CPUs according to the received action  $C_{p,v}^+$ . In case the vehicle  $v$  is processed by another PoP (i.e.,  $p'_v \neq$

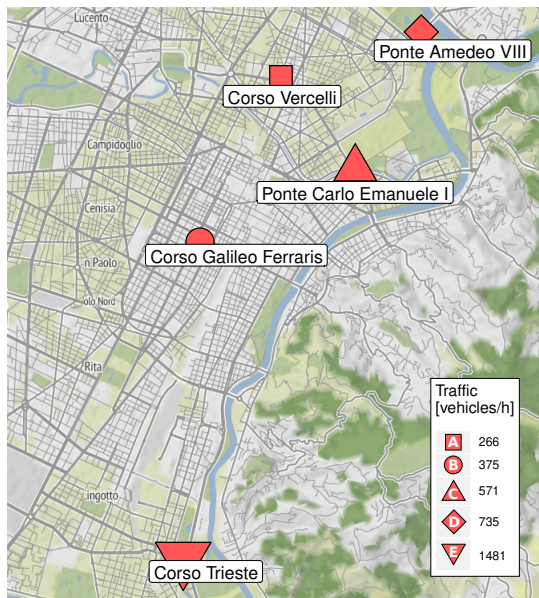


Fig. 5: PoPs across Turin with the average car traffic load.

$p_v$ ) the *environment* accounts for the transmission delay that vehicle  $v$  will experience; the delay overhead is set to  $l_{p_v, p'_v} = 20$  ms, which equals to two times the one-way E2E latency (i.e., UL+DL) for 5G networks [1] [58] (as shown in formula (4)).

- v) The *environment* iterates over each *PoP queue* and computes the reward per PoP  $R(s_{v,p}, a_v)$  using formula (11) and vehicles' experienced delay given by formula (4). Then, the average reward by all PoPs is sent to the agents  $\frac{1}{P} \sum_{p \in P} R(s_{v,p}, a_v)$ . Maximizing this average reward is the goal of the MDP described in Problem 2.

The steps above are summarized in Algorithm 2. In the next section, we detail the dataset used to obtain the arrival time of vehicles  $t_v$ , and each vehicle's associated PoP  $p_v$ .

### B. Vehicular Mobility Dataset

In order to feed the environment with realistic traffic we collected a dataset spanning from January to October 2020 of vehicle traffic gathered in Turin (Italy). There are over 100 measuring locations distributed throughout Turin where the number of vehicles that pass each particular measuring point is counted over 5 minute intervals. At the end of every interval, the traffic intensity (i.e., the number of vehicles arriving in that 5 minute interval divided by 5 minutes) is expressed as a number of vehicles per hour. Not all measuring points do report traffic intensities for each 5 minute interval, hence we interpolate the missing measurements via expectation maximization. Additionally, we consider  $P = 5$  PoPs to find optimal solutions of Problem 1 using commodity solvers in Section VI-C4. For  $P > 5$ , finding optimal solutions becomes intractable due to the fast growth of the search space in Problem 1. Fig. 5 shows how the measuring points (which we consider to be as PoPs) are distributed across the city.

This dataset provides us the traffic intensity  $\Lambda_p(t)$  [vehicles/hour] at each PoP  $p \in \{1, \dots, P\}$  every

TABLE III: Training and testing traces.

trace	start	end	duration	arrivals
training	Jan 28 17:55	Jan 29 07:13	13.3 hrs	28352
testing	Jan 29 07:13	Jan 29 12:43	5.5 hrs	28353

5 minutes. We use these time-varying  $\Lambda_p(t)$  values as the arrival rates of  $P$  independent Poisson processes that model vehicle arrivals on instants  $t_v$  at the  $P$  PoPs. Namely, at each time window  $[t, t + 5\text{min}]$  we iterate over each PoP  $p$  and randomly generate its car arrivals as

$$\{t_1, t_2, \dots\} = \{t_i\}_i = \left\{ t + \sum_{j=0}^i k_j \right\}_i, \quad k_j \sim \text{Exp}(\Lambda_p(t)) \quad (17)$$

with  $\text{Exp}(\Lambda_p(t))$  denoting the exponential distribution with rate  $\Lambda_p(t)$ . By repeating this random generation of arrivals for every PoP  $p \in P$ , and for every time window of 5 min; we generate a dataset with samples  $\{(t_1, p_1), (t_2, p_2), \dots\}$  (time  $t_v$  of vehicle arrival at PoP  $p_v$ ). To gain statistical significance, we repeat 40 times the random generation of arrivals, using formula (17) with different seeds. As a result, we obtain 40 different traces that express how vehicles arrive to each PoPs in Fig. 5 between the 28<sup>th</sup> of January 2020, and the 1<sup>st</sup> of October 2020.

Remark that the considered PoPs exhibit increased traffic intensity  $\Lambda_p(t)$  during morning and afternoon rush hours, a pattern also observed in datasets from other cities, such as PeMSD4 (San Francisco Bay Area), PeMSD7 (District 7 of California), and PeMSD8 (San Bernardino) [59]–[61]. Consequently, the performance of DHPG evaluated in Section VI is expected to generalize to these cities. Specifically, DHPG can capture diverse traffic trends, as seen in the PeMSD7(L) dataset [61], provided it is trained on the corresponding traffic data during the training phase.

## VI. PERFORMANCE EVALUATION

In this section we evaluate the performance of the proposed approach on the task placement and scaling problem. Specifically, we study the performance of the DHPG as well as the decentralized scaling approach DDPG (as shown in Fig. 4), and compare them against other state-of-the-art scaling approaches. For the sake of simplicity, we denote the solutions using their associate scaling methods, as they share the same greedy-based placement strategy defined in formula (18).

### A. Comparison Solutions

We compare DHPG to fully or partially decoupled solutions, where the placement decision is followed by scaling, as presented in [7]. Specifically, we employ a greedy placement algorithm placing vehicle  $v$  tasks to the PoP  $p'_v$  that minimizes the average experienced delay, i.e., the transmission and processing latency:

$$p'_v = \underset{p \in P}{\text{argmin}} (\mathbb{E}[l_{p_v, p}] + \mathbb{E}[d_p]) \quad (18)$$

Scaling is tackled with the following approaches [7], [8] [9]:

- **Constant (CNST)** approach as baseline in which the number of active CPUs is constant over time. Exhaustive search is used to determine the number of CPUs per PoP that brings the highest reward on the training set  $V'$ :

$$\operatorname{argmax}_{(C_1, \dots, C_P)} \sum_{v \in V'} R(C_p, p'_v, t_v) \quad (19)$$

Note that  $C_{p,v} = C_p$ ,  $\forall v \in V'$  with  $C_p$  a constant.

- **Proportional Integral (PI)** controller [62], with parameters  $\alpha$  and  $\beta$ , that aims to keep the most loaded CPU below a selected threshold of  $\rho$  [8];
- **Triple Exponential Smoothing (TES)** scaling algorithm, that is an adaptation of the *n-max* solution in [9], that creates an equally spaced time series  $f_{p,t-S}, \dots, f_{p,t-1}, f_{p,t}$  corresponding to the flow (i.e., the number of vehicles) that each PoP  $p$  has received in the last  $S$  slots, each of  $m = 5$  minutes. Based on this flow time series, the algorithm uses TES [14] to predict the maximum traffic flow in a window of  $W \cdot m$  minutes, with  $W$  being the number of time slots to forecast. Then, the number of CPUs at each PoP  $p$  is scaled according to the TES forecast.
- **Deep Deterministic Policy Gradient (DDPG)** is a model-free, off-policy reinforcement learning algorithm that operates in environments with continuous action spaces [52]. It utilizes an actor-critic architecture, where the actor learns a deterministic policy that maps states to actions, while the critic estimates the expected cumulative future reward given a state and action. Authors in [7] proposed DDPG-DOD, a variant of DDPG, which exploits the underlying structure of the discrete action space, enabling more efficient learning and improving scalability in resource scaling problems. DDPG-DOD is referred to hereafter as DDPG for simplicity.

## B. Experimental Setup

All solutions are evaluated with the simulation environment presented in Section V, where we use Python 3.9.12, complemented with the PyTorch 1.11.0 library. We employ the data-set described in Section V-B in an area of 5 PoPs. To run the experiments we use a server with Intel Core i7-10700K CPU, 32 GB of RAM.

1) *Hyperparameters*: In the following, we give the detailed parameter settings for the algorithms mentioned in Section IV and VI-A.

**CNST**. We perform a grid search to find the optimal number of CPUs for the selected PoPs (five in total) in formula (19), namely sweeping over  $C_p$  where  $p \in \{1, 2, 3, 4, 5\}$ , resulting in  $6^5 = 7776$  combinations. The best found combination over the training set is  $(C_A, C_B, C_C, C_D, C_E) = (1, 5, 5, 1, 5)$ .

**PI**. We perform a grid search to find the optimal parameters  $\alpha$ ,  $\beta$  and  $\rho_{tgt}$  within the ranges suggested by the authors in [8]. The best found result over the training set is  $(\alpha, \beta, \rho_{tgt}) = (4, 0, 0.7)$ .

**TES**. TES is an adaptive algorithm that does not have a training phase. We set  $W \cdot m = 1$  second.

**DDPG**. The architectures of actor and critic are both a 3-layer perceptron. Each layer contains 64 neurons, followed by Exponential Linear Unit (ELU) [63] activation functions. The

size of replay buffer consists of  $1 \times 10^6$  entries; the discount factor is set to  $\gamma = 0.99$ ; the soft update for Polyak averaging is set to  $\tau = 1 \times 10^{-3}$ . Adam optimization [64] is employed with different learning rates  $\alpha_a = 1 \times 10^{-4}$  and  $\alpha_c = 1 \times 10^{-3}$  for the actor and critic, respectively, following the settings in [52]. Furthermore, a noise perturbation drawn from Gaussian distribution with  $\mu = 0$ ,  $\sigma = 0.1$  is introduced to the action value during training, to encourage exploration [65]. The model converges after 20 training episodes.

**DHPG**. The architectures of the actor  $\mu$ , critic  $Q$  and the hyper-parameters are similar to that of DDPG with minor differences: each layer contains 256 neurons, and the last layer of the actor split into two parallel action heads. In particular, the actor is composed of (i) a 3-layer perceptron as the joint state state encoder  $\mu_e$ , followed in parallel by (ii) a 2-layer perceptron as continuous head  $\mu_C$ ; and (iii) a 2-layer perceptron acting as discrete head  $\mu_p$ . The model converges after 30 episodes of training.

2) *Evaluation scenarios and metrics*: Our goal is to maximize the long term reward as described in formula (16) that aims at meeting the delay target without over-provisioning resources, by finding an adequate strategy for task placement and scaling over time.

**Convergence of DHPG**. We show the evolution of the long-term *average reward* as we increase the training episodes of the DHPG scaling agents.

**Comparison Analysis**. We run the approaches specified in Section VI-A using the traces summarized in Table III, and compare them on the basis of the (i) *average reward*, (ii) *number of active CPUs*, and (iii) *experienced delay*. Note that we consider a trace that is long enough to cover various traffic patterns, including peak/off-peak hours. To have statistical significance in our results, we use 40 different traces (see Section V-B) for each experiment that span through the training or testing period.

**DHPG vs DDPG per PoP**. We closely examine the behavior of the DHPG and DDPG algorithms at each PoP to analyze how the agents distribute the *workload*.

**Optimality Gaps**. We show the optimality gap with regards to the global optimal solution for Problem 1.

**Computational Complexity**. Finally, we investigate the computational complexity of the proposed approaches and compare them against the state-of-the-art solutions.

## C. Results

1) *Convergence of DHPG*: Fig. 6 shows the learning curve of DHPG over 30 episodes. We report average rewards and the corresponding 95% confidence intervals by repeating the experiment 10 times.

We can see that DHPG converges in around 5 episodes, and the subsequent episodes lead to rather small increase in the achieved reward. Fig. 6 also shows that the training reward is smaller than the testing reward, as DHPG placement decisions are taken by the discrete action head  $\mu_p$ , via sampling actions based on the a probability distribution. That is, during the training stage DHPG forwards the vehicle task to a stochastic PoP obtained through  $p'_v = X(\mu_p(z_v | \theta^\mu))$  – see line 13 from

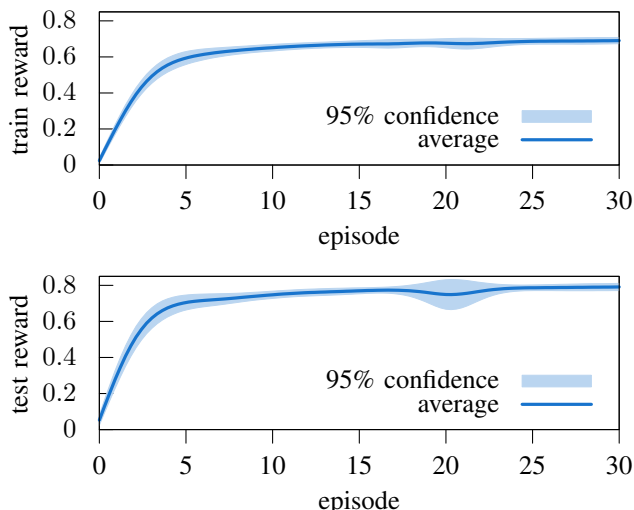


Fig. 6: DHPG learning curves over the training and testing sets.

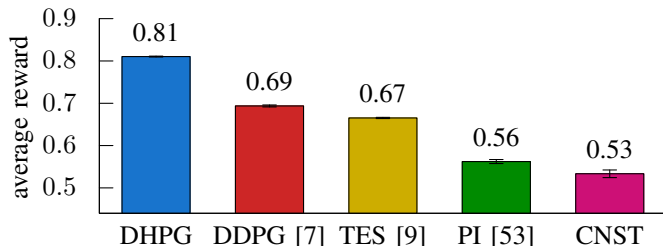


Fig. 7: Average reward over 40 traces (generated with different random seeds) of a 5.5h interval. Number annotations represent the average value, and error bars represent three times the standard deviations.

Algorithm 1. Whereas during the testing stage, the DHPG agent selects the PoP with the maximum likelihood.

In Fig. 6 we also observe how the confidence interval of the reward grows at episode 20. In the testing traces we observe that in one out of ten runs, the DHPG exhibits a sudden reward drop/increase. Such effect may be caused by (i) outliers in task departure times  $T_v$ , which are randomly generated at each run based on the process specified in Section V-A; or (ii) not having a sufficiently small learning rate  $\alpha_a$ . Nevertheless, the reward at the training and testing traces remain stable in the long run.

2) *Comparison Analysis*: We compare the DHPG agent with the solutions in Section VI-A. The comparison is done over the 40 randomly generated periods of 5.5h in the testing trace – Formula (17) and Table III, respectively. Fig. 7 illustrates the reward for each approach averaged over the 40 versions of the testing trace, while the error bars show three times the associated standard deviation of the reward.

We can see that DHPG and DDPG obtain higher average rewards by 13% and 2% compared to the one attained by TES, respectively; while PI and CNST remain below TES with a decrease in average reward of 11% and 14%, respectively. Moreover, the behaviour of almost every solution is fairly

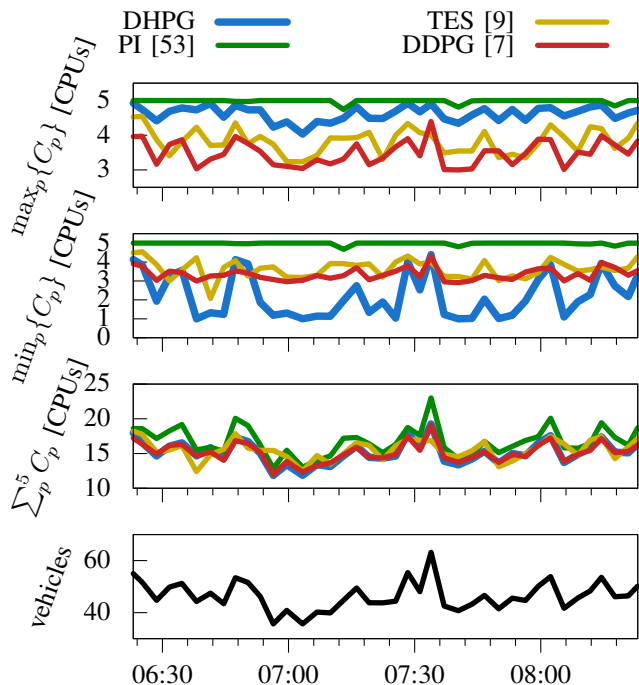


Fig. 8: Behaviour of DHPG and other solutions as the number of vehicles change over time (bottom). From top to down we show the maximum/minimum CPUs each PoP has ( $\max_p\{C_p\}$  and  $\min_p\{C_p\}$ , respectively), and the sum of PoP CPUs ( $\sum_p^5 C_p$ ).

stable (see the error bars in Fig. 7) thanks to the training approach used; the parameters of every solution are selected to maximize the reward for a training trace with both off-peak and rush hours during the day. Hence, every solution generalizes adequately despite the traffic variations of the 40 different versions of the testing trace.

To understand the rewards reported in Fig. 7 we take a look at the behaviour of every solution during rush hours in the city of Turin. In Fig. 8, we omit the CNST case, which we used as a benchmark in Fig. 7, to render the figure more readable. To further increase its readability, we smooth the traces by using Bezier curves to capture the main trends without being distracted by the small fluctuations inherent to the traces.

We first focus on the PI approach. Primarily, PI obtains a small reward due to its failure to distribute the C-V2N traffic among PoPs, since there is almost always a PoP with 5 active CPUs ( $\max_p\{C_p\} = 5$  during long periods in Fig. 8). A second reason is that PI has the highest number of CPUs ( $\sum_p C_p$ ) across PoPs. And the third reason is that PI leads to the largest increase of CPUs upon traffic peaks. Fig. 8 shows that as road traffic peaks around 7:30, it leads to the highest number of active CPUs ( $\sum_p C_p > 20$ ). PI is over-provisioning computing resources, as a conservative solution that aims at keeping load around 0.7 – the best found target load for the  $d_{tgt}$  parameter, as described in Section VI-B1.

Although Fig. 8 conveys the flaws of PI, it does not readily reveal why DHPG and DDPG outperform TES. Actually, the three solutions use almost the same number of CPUs across PoPs  $\sum_p C_P$ . The main difference is that DHPG is prone

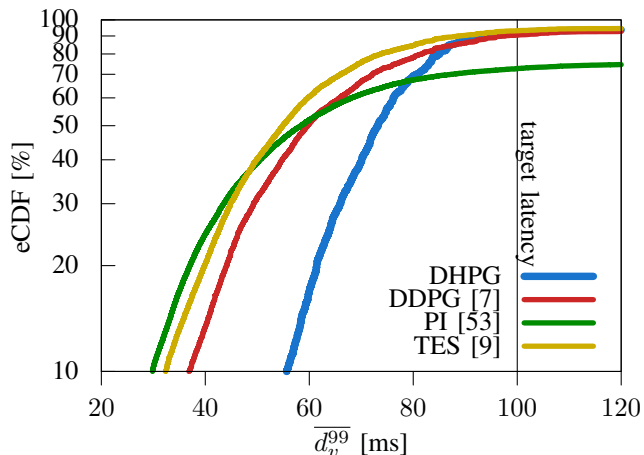


Fig. 9: eCDF for the upper bound of the 99 delay percentile.

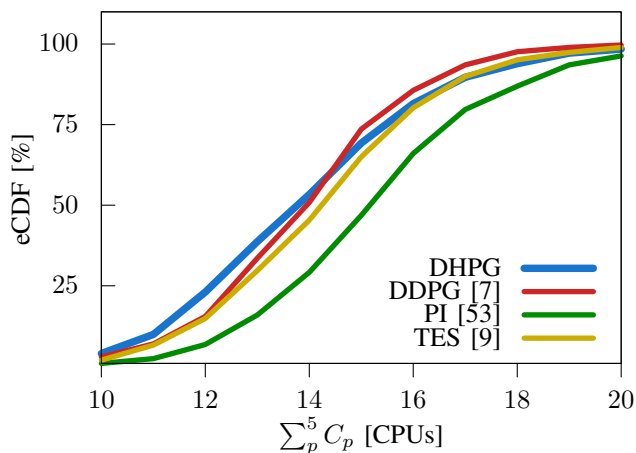


Fig. 10: eCDF of CPUs used by all PoPs  $\sum_p C_p$ .

to consolidating workloads at certain PoPs. We observe that the number of CPUs for the most loaded PoP ( $\max_p \{C_p\}$ ) remains higher than for DDPG and TES (see Fig. 8 top). At the same time, DHPG tends to have less CPUs in the least loaded PoP ( $\min_p \{C_p\}$ ) compared to DDPG and TES.

To gain a deeper understanding on the behaviour of DHPG and other benchmarks, we plot (i) the Empirical Cumulative Distribution Function (eCDF) of the delay  $d_v^{99}$  experienced by vehicles in Fig. 9 and (ii) the eCDF of the total number of active CPUs across the five PoPs in Fig. 10. For the former we compute the average delay experienced over time in the experiments, and then compute the 99-percentile bound from formula (6).

Fig. 9 shows that with DHPG the 99<sup>th</sup> percentile of the delay remains close to the target of 100 ms, violating the delay constraint at approximately 10% of the times (similar as TES and DDPG), while DDPG and TES result in smaller task delays. In line with the previous figure, Fig. 10 shows that DHPG uses less CPUs to ensure the target delay. In particular, DHPG has higher chances than TES and DDPG to use less than 14 CPUs, thus achieving a higher reward in Fig. 7.

Overall, Fig. 9 and Fig. 10 show a rather similar behaviour for TES and DDPG. The proposed DHPG ends up outperform-

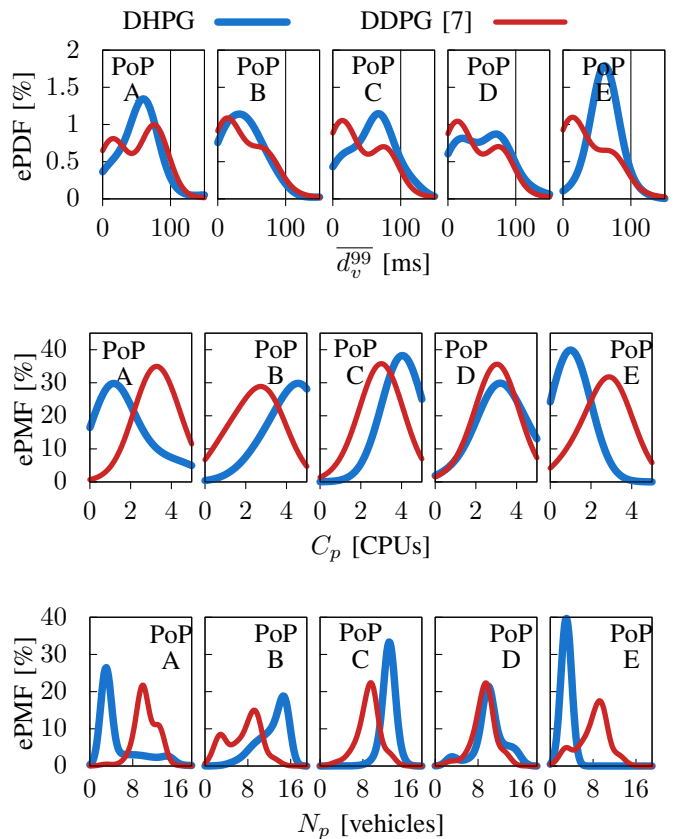


Fig. 11: Comparison of DHPG vs. DDPG over all PoPs. We compare the ePDF of the 99 delay percentile bound  $d_v^{99}$  (top), ePMF of the number of CPUs  $C_p$  at each PoP (middle), and number of vehicles assigned to each PoP  $N_p$  (bottom).

ing all the solutions because it is more likely to use less CPUs while ensuring that 99<sup>th</sup> percentile of the delay remains below the 100 ms target. Both facts suggest that DHPG actor  $\mu$  has inherently learned the traffic trends at all PoPs, hence, placing new task arrivals at non-saturated PoPs to avoid turning on additional CPUs.

3) *DHPG vs DDPG per PoP*: In Fig. 11 we compare the behaviour of DHPG and DDPG per PoP on (i) the Empirical Probability Density Function (ePDF) of the the 99<sup>th</sup> percentile latency; (ii) the Empirical Probability Mass Function (ePMF) of the number of CPUs  $C_p$ ; and (iii) ePMF of the number of assigned vehicles  $N_p$ . As before, we use kernel density estimates to derive the ePDF and ePMFs.

Fig. 11 shows that DDPG distributes the number of vehicles  $N_p$  per PoP more evenly than DHPG, as the highest ePMF peak is near  $N_p = 8$  for every PoP. In comparison, DHPG assigns less vehicles to PoPs A and E, and more vehicles to PoPs B and C – see Fig. 11 (middle). Furthermore, we can see in Fig. 11 (top) that C-V2N tasks experience a larger delay at PoPs where DHPG dispatches fewer tasks – i.e. PoPs A and E. This is due to the significantly smaller number of CPUs used in PoPs A and E (Fig. 11 (middle)). With the use of DDPG, tasks experience a rather equally distributed latency (Fig. 11 (top)) as the approach distributes equally the load across PoPs. Finally, in terms of violating the 100 ms delay

TABLE IV: Small scale evaluation

Algorithm	avg gap	avg #CPUs	avg load
Oracle	-	3.20	86.6%
DHPG	5.2%	3.23	90%
PI	10.4%	3.04	89%
TES	11.3%	3.04	89%
DDPG	12.1%	3.02	89.2%
CNST	77.7%	3.40	77.4%

bound (Fig. 11 (top)), the two approaches behave quite similar, as already noted for Fig. 9.

Overall, Fig. 11 highlights that decentralized DDPG leads to a more even load distribution across PoPs. While DHPG manages to significantly ease the load at PoPs A and E, at the expense of loading more PoPs B and C. Still, the load ease at PoPs A and E is so significant – see Fig. 11 – that the total number of used CPUs turns out to be smaller with DHPG than with DDPG. Thus, DHPG outperforms DDPG regarding average reward in Fig. 7.

4) *Optimality Gap*: We study how far DHPG is with respect to the performance of optimal solution for Problem 1. To find an optimal solution we resort to an oracle that knows *a posteriori* the vehicle arrival times  $\{t_1, t_2, \dots\}$ . However, an oracle cannot solve Problem 1 in polynomial time – see Lemma 1. Hence, it is a must to reduce the problem size to find a feasible solution. The problem size is governed by the number of vehicle arrivals  $|V|$  considered, for the arrival of each vehicle  $v \in V$  is associated with the corresponding placement  $p'_v$  and scaling  $C_{p,v}$  decisions. In particular, there are  $(P(C_p^{\max})^P)^{|V|}$  possible decisions for a problem with  $|V|$  vehicle arrivals, i.e. a vast search space to find an optimal solution. For example, an oracle solution using AMPL [66] and the KNITRO [67] solver could not find a solution in 65 h for  $|V| = 81$  vehicle arrivals.

In order to find an optimal solution through an oracle we study a small scale instance of Problem 1. The considered small scale scenario concerns  $|V| = 6$  vehicle arrivals  $\{t_{v'}, \dots, t_{v'+6}\}$  and a common starting system state  $s_{v'}$ . The system state corresponds to the one achieved by DHPG by the time  $t_{v'}$  vehicle  $v'$  arrived.

Table IV shows the optimality gap achieved by DHPG and the benchmarks in the aforementioned small scale scenario. The optimality gap is measured as the relative difference between the oracle reward  $R^*$  and the reward achieved by the algorithm  $R$ , i.e. we compute it as  $\frac{R^* - R}{R^*}$ . Clearly, DHPG is the one staying the closest to the optimal solution, with just a 5.2% optimality gap. Whereas, DDPG and other benchmarks have optimality gaps above a 10%. Although TES and PI outperform DDPG in the considered small scale scenario, the latter achieves larger long-term reward – see Fig. 7.

Table IV also details that all solutions use around three CPUs. Such result is because with three CPUs it is possible to achieve task processing delays close to the target delay  $d_{tgt}$  (see Fig. 12), thus leading to higher reward. It is worth to mention that DHPG fosters task delays *close* to the target  $\min d_v - d_{tgt}$ , whereas the benchmarks foster task delays *below* the target latency  $d_v < d_{tgt}$  due to their greedy placement (18) strategy. As a result, DHPG may lead to under-

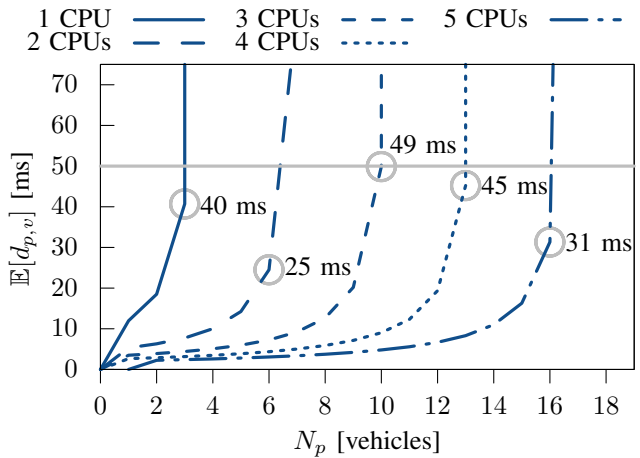


Fig. 12: Experienced average processing delay  $\mathbb{E}[d_{p,v}]$  at a PoP as the number of assigned vehicles  $N_p$  and CPUs (lines) increase.

TABLE V: Computational complexity of algorithms.

DHPG	DDPG	PI	TES
$\mathcal{O}(\eta^2 H)$	$\mathcal{O}(\eta^2 H)$	$\mathcal{O}(P)$	$\mathcal{O}(P)$

provisioning of PoP yet with high rewards. This aligns with the fact that DHPG has higher load and CPUs than the benchmarks in Table IV.

Overall, we conclude that by leveraging a data-driven approach, DHPG learns a more flexible strategy in placement dimension, rather than using greedy method. The design of joint state encoder effectively exploits the inter-dependency between placement and scaling to maximize the reward.

5) *Computational Complexity*: In this section, we derive the worst-case computational complexity analysis of the considered approaches.

PI, TES and DDPG take the placement decisions based on (18). Hence, the placement has computational complexity  $\mathcal{O}(P)$ . Then, TES performs  $W$   $m$ -minutes predictions at each PoP to decide upon scaling, having an overall computational complexity  $\mathcal{O}(WP)$ . PI performs a fixed set of operations at each PoP to derive the scaling decision, thus having a runtime complexity  $\mathcal{O}(P)$ . DDPG uses its trained DDPG actor  $\mu$  to scale resources, as described in [7]. Each fully connected layer of the actor network performs a vector-matrix multiplication  $\mu_i \cdot h_{i-1}$  during the forward pass, where  $\mu_i \in \mathbb{R}^{\eta_i \times \eta_i}$  are the weights of the  $i^{\text{th}}$  hidden layer with  $h_i$  neurons,  $\eta_i$  being the number of neurons at the  $i^{\text{th}}$  hidden layer, and  $h_{i-1} \in \mathbb{R}^{\eta_i}$  being the output of the previous layer. Let  $\eta = \max_i \{\eta_i\}$  denote the maximum number of neurons in any hidden layer and  $H$  for the total number of hidden layers. Then a forward pass of the DDPG actor network  $\mu$  has a computational complexity of  $\mathcal{O}(\eta^2 H)$ . Since the forward pass dominates the placement operation, which has complexity  $\mathcal{O}(P)$ , this also determines the overall complexity of the DDPG agent.

The DHPG framework constitutes of a joint actor and a joint critic, as illustrated in Fig. 3. To obtain the computational

complexity of DHPG at *inference stage*, we look into the operations performed by the joint actor  $\mu$ . The input state vector  $s_v$  traverses 5 fully connected hidden layers, each with  $\eta_i$  neurons. Every layer has a weight matrix  $\mu_i \in \mathbb{R}^{\eta_i \times \eta_{i-1}}$  and performs a vector-matrix multiplication  $\mu_i \cdot h_{i-1}$ , with  $h_i \in \mathbb{R}^{\eta_i}$  being the size of a hidden layer. Hence, the computational complexity of a forward pass in the joint actor corresponds to one matrix multiplication per layer, i.e.,  $\mathcal{O}(\eta^2 H)$  with  $\eta = \max_i \{\eta_i\}$ . The last layer of the joint actor has as many neurons as PoPs. As a result, an increasing number of PoPs  $P$  will lead to a longer inference time.

To obtain the computational complexity of DHPG at the *training stage*, we look into the operations performed by the joint critic  $Q$  and recall the learning Algorithm 1. The joint critic  $Q$  has three fully connected hidden layers with the last layer estimating the  $Q$ -value. The first hidden layer receives the state-action tuple  $(s_v, a_v)$  and has a weight matrix  $\theta_1^Q \in \mathbb{R}^{\eta_1 \times (3P+2)}$ , with  $P$  being the number of PoPs and  $\eta_1$  being the number of neurons of the layer. Hence, a forward pass of the first layer has computational complexity  $\mathcal{O}(\eta_1 P)$ . Performing a forward pass across all five layers involves the matrix multiplication of the weights associated to each layer, with the inner layers having weight matrix  $\theta_i^Q \in \mathbb{R}^{\eta_i \times \eta_{i-1}}$ . Therefore, the computational complexity of critic  $Q$  is  $\mathcal{O}(\eta^2 H)$  with  $\eta = \max\{\eta_i, 3P + 2\}$ . Considering Algorithm 1, the dominant operation at the training stage is the update of the critic  $\delta\theta^Q$  and actor  $\delta\theta^\mu$  weights using the batch of  $b$  transitions of the replay buffer. To compute the critic update  $\delta\theta^Q$  we calculate the mean square error between the critic  $Q$  and target critic  $Q'$  for each sample within the batch, i.e., we perform  $2b$  forward passes for the critic and target critic – that is  $\mathcal{O}(b\eta^2 H)$  operations. Then, we run a back propagation to compute the associated gradient descend  $\nabla_{\theta^Q}$  in line 21. As the complexity of the back propagation is defined by a matrix multiplication for each layer [68], computing  $\delta\theta^Q$  has a total complexity of  $\mathcal{O}(b\eta^2 H)$ . Similarly, the complexity of the critic update  $\delta\theta^\mu$  is  $\mathcal{O}(b\eta^2 H)$ . As a result, the overall complexity of DHPG at its training stage is  $\mathcal{O}(EVb\eta^2 H)$  with  $E$  being the number of episodes and  $V$  being the number of vehicle arrivals in the training dataset.

In summary, the computational complexity of the DHPG is determined by the number and size of hidden layers, as well as training hyper-parameters, including episodes, batch size, and training dataset size. Increasing the number of PoPs will linearly increase the runtime of the forward pass for the last layer of the actor and the first layer of the critic, respectively.

Overall, the DDPG and DHPG solutions have higher computational complexity, as shown in Fig. 13, which illustrates the average runtime of each algorithm for the experiments conducted in Sub-sections VI-C1-VI-C3. Nevertheless, they still achieve runtimes in the sub-msec range. Thus, the proposed DHPG solution is suitable for C-V2N services with strict latency requirements. Note that taking  $\leq 500 \mu\text{s}$  to perform the placement and scaling is fast enough for C-V2N services with down to  $d_{tgt} = 10$  ms latency requirements – not to mention the considered service in Section VI, with  $d_{tgt} = 100$  ms.

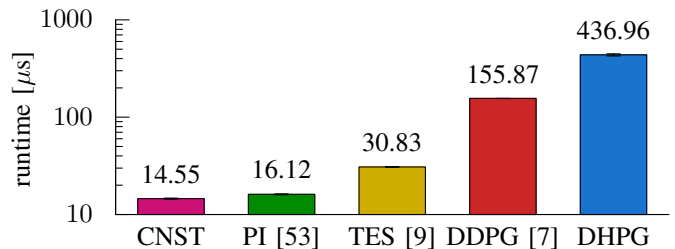


Fig. 13: Average runtime of each algorithm when performing the placement and scaling in the considered 5 PoPs upon the arrival of a vehicle.

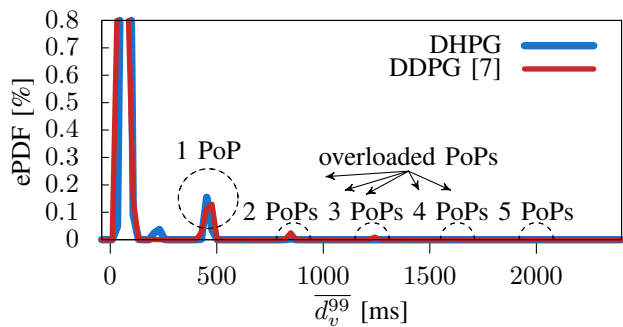


Fig. 14: Tail of the ePDF for vehicles' 99-percentile latency bound  $\overline{d}_v^{99}$ . Prominent peaks on DDPG are due to CPU overload  $\rho_p > 1$  on multiple PoPs.

#### D. Discussion on Reward Function

We hereby discuss the implications of the evaluation of the proposed approach for task placement and scaling of edge resources. Namely, we discuss how the reward function impacts the optimality gap, and how to reshape it to further boost DHPG performance.

The optimality gap of DHPG may be attributed to the design of the reward function in formula (11), which does not decay fast when the experienced delay exceeds the target – see  $d > d_{tgt}$  values in Fig. 2. Although the DHPG agent learns to meet the target 99 delay percentile  $d = d_{tgt}$ , we can still observe extreme values for the 99 delay percentile (with very small probability) – as the prominent peaks indicate in Fig. 14. We

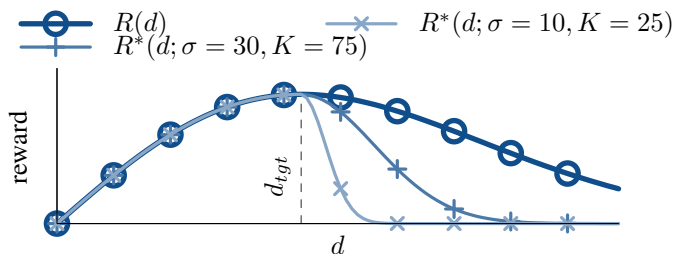


Fig. 15: Candidate rewards for future work  $R^*(d; \sigma, K)$ , and the reward  $R(d)$  used in our experiments.  $R^*(d; \sigma, K)$  alike rewards will punish more the under-provisioning, i.e.  $d > d_{tgt}$ .

argue that a faster decay in the reward for  $d > d_{tgt}$  may reduce the chances of overloading, thus preventing delay violations. In this direction the following reward function is provided as an example, also illustrated in Fig. 15.

$$R^*(d; \sigma, K) = \begin{cases} R(d), & d < d_{tgt} \\ \frac{K}{\sigma} \frac{\phi\left(\frac{d-d_{tgt}}{\sigma}\right)}{\Phi\left(\frac{b-d_{tgt}}{\sigma}\right) - \Phi\left(\frac{a-d_{tgt}}{\sigma}\right)}, & d \geq d_{tgt} \end{cases} \quad (20)$$

with  $d \geq d_{tgt}$  being a  $K$ -scaled truncated normal distribution [69] in the interval  $[a, b] = \mathbb{R}^+$ , centered at  $d_{tgt}$  with standard deviation  $\sigma$ ;  $\phi(x) = 1/\sqrt{2\pi} \exp(-\frac{1}{2}x^2)$ ; and  $\Phi(x) = \frac{1}{2}(1 + \text{erf}(x/\sqrt{2\pi}))$ . Note that the  $K$  scaling is set to ensure the reward continuity, i.e.  $\lim_{\varepsilon \rightarrow 0} R^*(d + \varepsilon; \sigma, K) = \lim_{\varepsilon \rightarrow 0} R^*(d - \varepsilon; \sigma, K)$ . Moreover,  $R^*(d; \sigma, K)$  is differentiable at  $d = d_{tgt}$  to help learning stability.

## VII. CONCLUSION

In this paper we studied C-V2N service provisioning supported by the edge cloud. More specifically, we propose a DRL approach for C-V2N application task placement and scaling of edge computing resources. Task placement refers to the discrete problem of placing application tasks associated to each vehicle to the most appropriate PoP. Resource scaling is dealing with discrete problem of scaling CPUs resources in each PoP, to efficiently support the C-V2N application tasks. As shown however in [7], we transfer the resource scaling problem to a continuous action space, to address the scalability issues inherent to the high-dimensional discrete action spaces. To optimize the cost-efficient utilization of edge resources and meet the delay constraints of the C-V2N service, application tasks associated with a vehicle entering a service area can be offloaded to any nearby PoP taking also into account the additional transmission latency. To tackle the two interdependent problems with heterogeneous action spaces, we propose DHPG, a deep reinforcement learning approach designed to handle hybrid action spaces. This enables DHPG to make holistic decisions that consider both task placement and resource scaling concurrently, leading to improved performance in C-V2N service provisioning.

We compare the performance of DHPG against state-of-the-art scaling algorithms, including a traditional PI controller, a forecast-based n-max approach (TES), and a DDPG-based approach, coupled with a greedy-based placement agent. DHPG demonstrates its capability to learn and exploit the inherent seasonality in the workload. This enables DHPG to adopt a more aggressive policy, resulting in performance improvements ranging from 17.4% to 52.8% against the considered state-of-the-art algorithms.

We further benchmarked DHPG against an oracle solution assuming knowledge of all future vehicle arrivals. Our proposed DHPG achieves an optimality gap of 5.2%, despite the fact that it relies solely on causal information. In future work, we will explore various reward functions associated with the target delay. Moreover, extensions of DHPG will be explored for handling correlated PoPs on a larger scale.

## ACKNOWLEDGEMENT

This work has been performed in the framework of the (i) Horizon SNS JU DESIRE6G (No. 101096466); (ii) National Growth Fund through the Dutch 6G flagship project ‘‘Future Network Services’’; and (iii) Remote Driver Project of the Spanish Ministry of Economic Affairs and Digital Transformation under Grant TSI-065100-2022-003;

## REFERENCES

- [1] ‘‘Technical Specification Group Services and System Aspects: Enhancement of 3GPP support for V2X scenarios,’’ 3GPP, Technical Specification 22.186.v17.0.0, April 2022.
- [2] M. H. C. Garcia, A. Molina-Galan, M. Boban, J. Gozalvez, B. Coll-Perales, T. Sahin, and A. Kousaridas, ‘‘A Tutorial on 5G NR V2X Communications,’’ *IEEE Communications Surveys Tutorials*, vol. 23, no. 3, pp. 1972–2026, 2021.
- [3] A. Rammohan *et al.*, ‘‘Revolutionizing intelligent transportation systems with cellular vehicle-to-everything (C-V2X) technology: Current trends, use cases, emerging technologies, standardization bodies, industry analytics and future directions,’’ *Vehicular Communications*, p. 100638, 2023.
- [4] 3GPP TS 23.28, ‘‘Architecture enhancements for V2X services (Release 16),’’ Tech. Rep., March 2019.
- [5] M. Ahmed, S. Raza, M. A. Mirza, A. Aziz, M. A. Khan, W. U. Khan, J. Li, and Z. Han, ‘‘A survey on vehicular task offloading: Classification, issues, and challenges,’’ *Journal of King Saud University - Computer and Information Sciences*, vol. 34, no. 7, pp. 4135–4162, 2022.
- [6] M. Noor-A-Rahim, Z. Liu, H. Lee, M. O. Khyam, J. He, D. Pesch, K. Moessner, W. Saad, and H. V. Poor, ‘‘6G for vehicle-to-everything (V2X) communications: Enabling technologies, challenges, and opportunities,’’ *Proceedings of the IEEE*, vol. 110, no. 6, pp. 712–734, 2022.
- [7] C. S.-H. Hsu, J. Martın-Perez, C. Papagianni, and P. Grosso, ‘‘V2N service scaling with deep reinforcement learning,’’ in *NOMS 2023-2023 IEEE/IFIP Network Operations and Management Symposium*, 2023, pp. 1–5.
- [8] D. De Vleeschauwer, J. Baranda, J. Manges-Bafalluy, C. F. Chiasserini, M. Malinverno, C. Puligheddu, L. Magoula, J. Martın-Perez, S. Barmounakis, K. Kondepudi, L. Valcarezhi, X. Li, C. Papagianni, and A. Garcia-Saavedra, ‘‘5Growth Data-Driven AI-Based Scaling,’’ in *2021 Joint European Conference on Networks and Communications 6G Summit (EuCNC/6G Summit)*, June 2021, pp. 383–388.
- [9] J. Martın-Perez, K. Kondepudi, D. De Vleeschauwer, V. Reddy, C. Guimaraes, A. Sgambelluri, L. Valcarezhi, C. Papagianni, and C. J. Bernardos, ‘‘Dimensioning V2N Services in 5G Networks Through Forecast-Based Scaling,’’ *IEEE Access*, vol. 10, pp. 9587–9602, 2022.
- [10] S. Verma and A. Bala, ‘‘Auto-Scaling Techniques for IoT-Based Cloud Applications: A Review,’’ *Cluster Computing*, vol. 24, no. 3, p. 2425–2459, sep 2021.
- [11] S. Rahman, T. Ahmed, M. Huynh, M. Tornatore, and B. Mukherjee, ‘‘Auto-Scaling VNFs Using Machine Learning to Improve QoS and Reduce Cost,’’ in *2018 IEEE International Conference on Communications (ICC)*, 2018, pp. 1–6.
- [12] T. Subramanya and R. Riggio, ‘‘Machine Learning-Driven Scaling and Placement of Virtual Network Functions at the Network Edges,’’ in *2019 IEEE Conference on Network Softwarization (NetSoft)*, 2019, pp. 414–422.
- [13] R. Li, Z. Zhao, Q. Sun, C.-L. I, C. Yang, X. Chen, M. Zhao, and H. Zhang, ‘‘Deep reinforcement learning for resource management in network slicing,’’ *IEEE Access*, vol. 6, pp. 74429–74441, 2018.
- [14] P. R. Winters, ‘‘Forecasting sales by exponentially weighted moving averages,’’ *Management science*, vol. 6, no. 3, pp. 324–342, 1960.
- [15] Y.-S. Lee and L.-I. Tong, ‘‘Forecasting time series using a methodology based on autoregressive integrated moving average and genetic programming,’’ *Knowledge-Based Systems*, vol. 24, no. 1, pp. 66–72, 2011.
- [16] A. Collet, A. Banchs, and M. Fiore, ‘‘LossLeap: Learning to Predict for Intent-Based Networking,’’ in *IEEE INFOCOM 2022 - IEEE Conference on Computer Communications*, 2022, pp. 2138–2147.
- [17] Z. Zhao, W. Chen, X. Wu, P. C. Y. Chen, and J. Liu, ‘‘LSTM network: a deep learning approach for short-term traffic forecast,’’ *IET Intelligent Transport Systems*, vol. 11, no. 2, pp. 68–75, 2017.
- [18] D. Bega, M. Gramaglia, M. Fiore, A. Banchs, and X. Costa-Perez, ‘‘AZTEC: Anticipatory Capacity Allocation for Zero-Touch Network Slicing,’’ in *IEEE INFOCOM 2020 - IEEE Conference on Computer Communications*, 2020, pp. 794–803.

- [19] Y. Fang, S. Ergüt, and P. Patras, "SDGNet: A Handover-Aware Spatiotemporal Graph Neural Network for Mobile Traffic Forecasting," *IEEE Communications Letters*, vol. 26, no. 3, pp. 582–586, 2022.
- [20] C. Zhang, H. Zhao, and S. Deng, "A density-based offloading strategy for IoT devices in edge computing systems," *IEEE Access*, vol. 6, pp. 73 520–73 530, 2018.
- [21] J. Du, L. Zhao, J. Feng, and X. Chu, "Computation offloading and resource allocation in mixed fog/cloud computing systems with min-max fairness guarantee," *IEEE Transactions on Communications*, vol. 66, no. 4, pp. 1594–1608, 2018.
- [22] K. Zhang, Y. Mao, S. Leng, Q. Zhao, L. Li, X. Peng, L. Pan, S. Maharjan, and Y. Zhang, "Energy-efficient offloading for mobile edge computing in 5G heterogeneous networks," *IEEE Access*, vol. 4, pp. 5896–5907, 2016.
- [23] C. Pradhan, A. Li, C. She, Y. Li, and B. Vucetic, "Computation offloading for IoT in C-RAN: Optimization and deep learning," *IEEE Transactions on Communications*, vol. 68, no. 7, pp. 4565–4579, 2020.
- [24] X. Zhao, K. Yang, Q. Chen, D. Peng, H. Jiang, X. Xu, and X. Shuang, "Deep learning based mobile data offloading in mobile edge computing systems," *Future Generation Computer Systems*, vol. 99, pp. 346–355, 2019.
- [25] N. Zhao, Y.-C. Liang, D. Niyato, Y. Pei, and Y. Jiang, "Deep reinforcement learning for user association and resource allocation in heterogeneous networks," in *2018 IEEE Global Communications Conference (GLOBECOM)*, 2018, pp. 1–6.
- [26] X. Zhang, A. Pal, and S. Debroy, "Deep reinforcement learning based energy-efficient task offloading for secondary mobile edge systems," in *2020 IEEE 45th LCN Symposium on Emerging Topics in Networking (LCN Symposium)*, 2020, pp. 48–59.
- [27] X. Chen, H. Zhang, C. Wu, S. Mao, Y. Ji, and M. Bennis, "Performance optimization in mobile-edge computing via deep reinforcement learning," in *2018 IEEE 88th Vehicular Technology Conference (VTC-Fall)*, 2018, pp. 1–6.
- [28] X. Liu, Z. Qin, and Y. Gao, "Resource allocation for edge computing in IoT networks via reinforcement learning," in *ICC 2019 - 2019 IEEE International Conference on Communications (ICC)*, 2019, pp. 1–6.
- [29] L. Huang, S. Bi, and Y.-J. A. Zhang, "Deep reinforcement learning for online computation offloading in wireless powered mobile-edge computing networks," *IEEE Transactions on Mobile Computing*, vol. 19, no. 11, pp. 2581–2593, 2020.
- [30] I. Ullah, H.-K. Lim, Y.-J. Seok, and Y.-H. Han, "Optimizing task offloading and resource allocation in edge-cloud networks: a DRL approach," *J. Cloud Comput.*, vol. 12, no. 1, Jul. 2023.
- [31] J. Yang, Q. Yuan, S. Chen, H. He, X. Jiang, and X. Tan, "Cooperative task offloading for mobile edge computing based on multi-agent deep reinforcement learning," *IEEE Transactions on Network and Service Management*, vol. 20, no. 3, pp. 3205–3219, 2023.
- [32] H. Jiang, X. Dai, Z. Xiao, and A. Iyengar, "Joint task offloading and resource allocation for energy-constrained mobile edge computing," *IEEE Transactions on Mobile Computing*, vol. 22, no. 7, p. 4000–4015, Jul. 2023.
- [33] S. Liu, J. Tian, C. Zhai, and T. Li, "Joint computation offloading and resource allocation in vehicular edge computing networks," *Digital Communications and Networks*, vol. 9, no. 6, pp. 1399–1410, 2023.
- [34] S. Li, N. Zhang, R. Jiang, Z. Zhou, F. Zheng, and G. Yang, "Joint task offloading and resource allocation in mobile edge computing with energy harvesting," *Journal of Cloud Computing*, vol. 11, no. 1, p. 17, 2022.
- [35] P. Lai, Y. Tao, J. Qin, Y. Xie, S. Zhang, S. Tang, Q. Huang, and S. Liao, "Joint optimization of application placement and resource allocation for enhanced performance in heterogeneous multi-server systems," *Computer Networks*, vol. 253, p. 110692, 2024.
- [36] T. Q. Dinh, J. Tang, Q. D. La, and T. Q. S. Quek, "Offloading in mobile edge computing: Task allocation and computational frequency scaling," *IEEE Transactions on Communications*, vol. 65, no. 8, pp. 3571–3584, 2017.
- [37] W. Zhou, W. Fang, Y. Li, B. Yuan, Y. Li, and T. Wang, "Markov approximation for task offloading and computation scaling in mobile edge computing," *Mobile Information Systems*, vol. 2019, no. 1, p. 8172698, 2019.
- [38] Z. Chen and X. Wang, "Decentralized computation offloading for multi-user mobile edge computing: A deep reinforcement learning approach," *EURASIP Journal on Wireless Communications and Networking*, vol. 2020, no. 1, pp. 1–21, 2020.
- [39] J. Chen, H. Xing, Z. Xiao, L. Xu, and T. Tao, "A DRL agent for jointly optimizing computation offloading and resource allocation in MEC," *IEEE Internet of Things Journal*, vol. 8, no. 24, pp. 17 508–17 524, 2021.
- [40] H. Peng and X. Shen, "Deep reinforcement learning based resource management for multi-access edge computing in vehicular networks," *IEEE Transactions on Network Science and Engineering*, vol. 7, no. 4, pp. 2416–2428, 2020.
- [41] Z. Nan, S. Zhou, Y. Jia, and Z. Niu, "Joint task offloading and resource allocation for vehicular edge computing with result feedback delay," *IEEE Transactions on Wireless Communications*, vol. 22, no. 10, pp. 6547–6561, 2023.
- [42] S. Wang, X. Song, H. Xu, T. Song, G. Zhang, and Y. Yang, "Joint offloading decision and resource allocation in vehicular edge computing networks," *Digital Communications and Networks*, 2023.
- [43] J. Huang, J. Wan, B. Lv, Q. Ye, and Y. Chen, "Joint computation offloading and resource allocation for edge-cloud collaboration in internet of vehicles via deep reinforcement learning," *IEEE Systems Journal*, vol. 17, no. 2, pp. 2500–2511, 2023.
- [44] Z. Sun, G. Sun, Y. Liu, J. Wang, and D. Cao, "Bargain-match: A game theoretical approach for resource allocation and task offloading in vehicular edge computing networks," *IEEE Transactions on Mobile Computing*, vol. 23, no. 2, pp. 1655–1673, 2024.
- [45] A. Islam, A. Debnath, M. Ghose, and S. Chakraborty, "A survey on task offloading in multi-access edge computing," *Journal of Systems Architecture*, vol. 118, p. 102225, 2021.
- [46] F. Malandrino, C. F. Chiasserini, G. Einziger, and G. Scalosub, "Reducing Service Deployment Cost Through VNF Sharing," *IEEE/ACM Transactions on Networking*, vol. 27, no. 6, pp. 2363–2376, 2019.
- [47] R. Cohen, L. Lewin-Eytan, J. S. Naor, and D. Raz, "Near optimal placement of virtual network functions," in *2015 IEEE Conference on Computer Communications (INFOCOM)*, 2015, pp. 1346–1354.
- [48] S. Agarwal, F. Malandrino, C.-F. Chiasserini, and S. De, "Joint VNF Placement and CPU Allocation in 5G," in *IEEE INFOCOM 2018 - IEEE Conference on Computer Communications*, 2018, pp. 1943–1951.
- [49] D. P. Heyman and M. J. Sobel, *Stochastic models in operations research. I. Stochastic processes and operating characteristics*. McGraw-Hill New York, NY, USA., 1982.
- [50] V. Mnih, K. Kavukcuoglu, D. Silver, A. Graves, I. Antonoglou, D. Wierstra, and M. Riedmiller, "Playing Atari with Deep Reinforcement Learning," 2013.
- [51] J. Zhu, F. Wu, and J. Zhao, "An overview of the action space for deep reinforcement learning," in *Proceedings of the 2021 4th International Conference on Algorithms, Computing and Artificial Intelligence*, 2021, pp. 1–10.
- [52] T. P. Lillicrap, J. J. Hunt, A. Pritzel, N. Heess, T. Erez, Y. Tassa, D. Silver, and D. Wierstra, "Continuous control with deep reinforcement learning," 2015.
- [53] "5GROWTH Scaling," <https://github.com/MartinPJorge/5growth-scaling/blob/master/FiftyStations/clean0326>, 2020.
- [54] R. S. Sutton and A. G. Barto, *Reinforcement learning: An introduction*. MIT press, 2018.
- [55] M. Alvarez-Mesa, C. C. Chi, B. Juurlink, V. George, and T. Schierl, "Parallel video decoding in the emerging HEVC standard," in *2012 IEEE International Conference on Acoustics, Speech and Signal Processing (ICASSP)*, 2012, pp. 1545–1548.
- [56] A. Shustanov and P. Yakimov, "CNN Design for Real-Time Traffic Sign Recognition," *Procedia Engineering*, vol. 201, pp. 718–725, 2017, 3rd International Conference "Information Technology and Nanotechnology", ITNT-2017, 25-27 April 2017, Samara, Russia.
- [57] "5G; Vehicle-to-everything (V2X); Media handling and interaction," ETSI, Sophia Antipolis - FRANCE, Standard, March 2020.
- [58] B. Coll-Perales, M. d. C. Lucas-Estañ, T. Shimizu, J. Gozalvez, T. Higuchi, S. Avedisov, O. Altintas, and M. Sepulcre, "End-to-End V2X Latency Modeling and Analysis in 5G Networks," January 2022.
- [59] Uppoor, Sandesh and Trullols-Cruces, Oscar and Fiore, Marco and Barcelo-Ordinas, Jose M, "Generation and analysis of a large-scale urban vehicular mobility dataset," *IEEE Transactions on Mobile Computing*, vol. 13, no. 5, pp. 1061–1075, 2013.
- [60] Gao, Haotian and Jiang, Renhe and Dong, Zheng and Deng, Jinliang and Ma, Yuxin and Song, Xuan, "Spatial-temporal-decoupled masked pre-training for spatiotemporal forecasting," *arXiv preprint arXiv:2312.00516*, 2023.
- [61] Fang, Yuchen and Qin, Yanjun and Luo, Haiyong and Zhao, Fang and Xu, Bingbing and Zeng, Liang and Wang, Chenxing, "When spatio-temporal meet wavelets: Disentangled traffic forecasting via efficient spectral graph attention networks," in *2023 IEEE 39th International Conference on Data Engineering (ICDE)*, 2023, pp. 517–529.

- [62] Kiam Heong Ang, G. Chong, and Yun Li, "PID control system analysis, design, and technology," *IEEE Transactions on Control Systems Technology*, vol. 13, no. 4, pp. 559–576, 2005.
- [63] D.-A. Clevert, T. Unterthiner, and S. Hochreiter, "Fast and Accurate Deep Network Learning by Exponential Linear Units (ELUs)," 2015.
- [64] D. P. Kingma and J. Ba, "Adam: A Method for Stochastic Optimization," 2014.
- [65] S. Fujimoto, H. van Hoof, and D. Meger, "Addressing Function Approximation Error in Actor-Critic Methods," 2018.
- [66] R. e. a. Fourer, "AMPL. A modeling language for mathematical programming," 1993.
- [67] R. A. Waltz and J. Nocedal, "KNITRO 2.0 User's Manual," pp. 33–34, 2004.
- [68] LeCun, Yann and Touresky, D and Hinton, G and Sejnowski, T, "A theoretical framework for back-propagation," in *Proceedings of the 1988 connectionist models summer school*, vol. 1, 1988, pp. 21–28.
- [69] Johnson, Norman L and Kotz, Samuel and Balakrishnan, Narayanaswamy, *Continuous univariate distributions*. John wiley & sons, 1995, vol. 289.
- [70] T. Öncan, "A survey of the generalized assignment problem and its applications," *INFOR: Information Systems and Operational Research*, vol. 45, no. 3, pp. 123–141, 2007.
- [71] G. I. Palmer, V. A. Knight, P. R. Harper, and A. L. Hawa, "Ciw: An open-source discrete event simulation library," *Journal of Simulation*, vol. 13, no. 1, pp. 68–82, 2019.

## APPENDIX A PROOF OF LEMMA 1

*Proof.* We proof the  $\mathcal{NP}$ -hardness of Problem 1 (Section 2.2) by showing that an instance of our problem is equivalent to the generalized assignment problem [70].

Let us consider an instance of Problem 1 that we want to solve for a time window  $T$ , in particular, we take a problem instance with every vehicle departing after the considered time window, i.e.,  $T_v > T$  holds  $\forall v$ .

When a vehicle  $v$  arrives to the vicinity of PoP  $p_v$  we have to take a *placement* decision to know that the C-V2N tasks of vehicle  $v$  will be processed at PoP  $p'_v$ . Note that the C-V2N tasks of vehicle  $v$  will induce a CPU increase  $C_{v,p'_v}^+$  at PoP  $p'_v$  to maximize the reward (i.e., to stay close to the target delay  $d_{tgt}$  in Fig. 2). Namely, the CPU increase is expressed as:

$$C_{v,p'_v}^+ = \underset{C}{\operatorname{argmax}} \{R(C, p'_v, N_{v-1,p'_v} + 1)\} - \underset{C}{\operatorname{argmax}} \{R(C, p'_v, N_{v-1,p'_v})\} \quad (21)$$

with  $N_{v-1,p'_v} + 1$  capturing that PoP  $p'_v$  will accommodate the tasks of an additional vehicle, i.e., vehicle  $v$ . Note how in formula (21) we make explicit the dependence on the number of vehicles  $N_{v,p'_v}$  within the reward function for the latter depends on the average processing delay  $d_{p,v}$  experienced by the vehicle, which is impacted by  $N_{v,p'_v}$  defined (Section 2.1) as:

$$\mathbb{E}[d_{p,v}] = \begin{cases} \frac{1}{\mu(C_{p,v}) - \lambda N_{p,v}} & \text{if } \mu(C_{p,v}) > \lambda N_{p,v} \\ \infty & \text{otherwise} \end{cases} \quad (22)$$

With the PoP CPU increase by each vehicle (21) we reformulate Problem 1 as:

$$\max_{p'_v} \sum_v \sum_p R(C_{p,v}, p'_v, N_p) \mathbb{1}_{p'_v}(p) \quad (23)$$

$$s.t. : \sum_v C_{v,p'_v}^+ \mathbb{1}_{p'_v}(p) \leq C_p^{\max}, \quad \forall p \quad (24)$$

$$p'_v \in P \quad (25)$$

We now indicate how the variables/parameters in the formulation above mimic to the notation used in the generalized assignment problem [70]. First, we take  $x_{v,p} = \mathbb{1}_{p'_v}(p)$  as the binary variable telling whether vehicle  $v$  C-V2N tasks are processed at PoP  $p$ . Second, we write  $R_{v,p} = R(C_p, p'_v, N_p)$  as the profit/reward obtained by having PoP  $p$  processing vehicle  $v$  C-V2N tasks. Third, we denote  $w_{v,p} = C_{v,p}^+$  as the CPU "weight" that vehicle  $v$  brings in to PoP  $p$  in terms of additional CPUs. Finally, we note that (25) means that every vehicle  $v$  C-V2N tasks must be processed at one PoP within the set  $P$ , i.e.,  $\sum_p x_{v,p} = 1$  must hold  $\forall v \in V$ . Overall, our reduction in (23)-(25) becomes:

$$\max \sum_v \sum_p p_{v,p} \cdot x_{v,p} \quad (26)$$

$$s.t. : \sum_v w_{v,p} \cdot x_{v,p} \leq C_p^{\max}, \quad \forall p \quad (27)$$

$$\sum_p x_{v,p} = 1, \quad \forall p \quad (28)$$

which is the generalized assignment problem with vehicles  $v$  being items that we have to place at a certain bins/PoPs  $p$ . In our case the profit is our reward function, and the bins' capacity is  $C_p^{\max}$ .

Therefore, we have found an instance of Problem 1 that is equivalent to the generalized assignment problem [70], which is  $\mathcal{NP}$ -hard. As a consequence, Problem 1 is also  $\mathcal{NP}$ -hard.  $\square$

## APPENDIX B TARGET LATENCY

In Section III we define the optimization Problem 1 to perform task placement and scaling. The reward function (11) is funded on the average processing latency – see the  $d_v$  term defined in (3). However, C-V2N services required that the target delay is met the  $\kappa$ -percent of the times.

To that end, in (6) we propose a bound for  $d_{p,v}^\kappa$  that relates the average and  $\kappa$  delay percentile. Specifically, the bound  $\overline{d_{p,v}^\kappa}$  uses  $K(\kappa)$ , a quantity that relates the average and  $\kappa$ -percentile as  $d_{p,v}^\kappa < K(\kappa) \cdot \mathbb{E}[d_{p,v}]$ . To find  $K(\kappa)$  we use the discrete event simulator CIW [71] as follows.

We run simulations for an M/D/1-PS queue that captures the deterministic processing times for video decoding/recognition [55], [56] in Advanced Driving tasks [1], [2]. Fig. 16 plots the ratio between the average delay (3) and the  $\kappa$  percentile of the delay using the service rates  $\mu$  reported in TABLE II. Results show that the 99-percentile of the delay is smaller than two times the average delay, i.e.  $K(99) = 2$ .

As a result, the experimental campaign in Section VI resorts to Lemma 2 to promote that DHPG agents meet the Advanced Driving requirement (i.e.  $d_{tgt} = 100$  ms) the 99% of the times. In particular, DHPG is trained with  $d_{tgt}$  replaced by  $\frac{d_{tgt}}{K(99)} = 50$  ms in the reward function (11). Consequently, DHPG demonstrably meets the 100 ms delay 99% of the time.

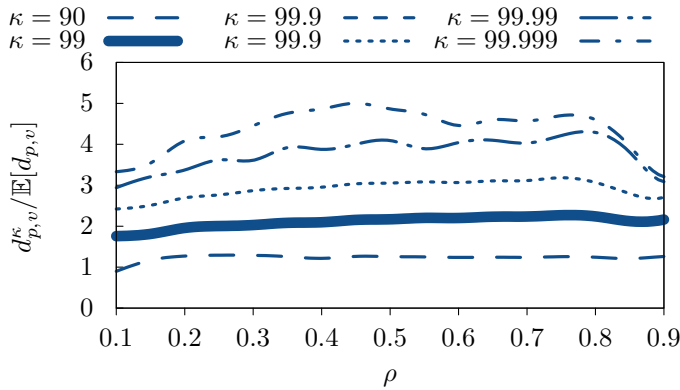


Fig. 16: Ratio of M/D/1-PS percentile latency  $d_{p,v}^{\kappa}$  and M/G/1-PS average latency  $\mathbb{E}[d_{p,v}]$  as the CPU load  $\rho$  increases. Results are obtained with the CIW simulator [71].



**Cyril Shih-Huan Hsu** is a Ph.D. candidate at the Informatics Institute, University of Amsterdam (UvA), The Netherlands, where he has been pursuing his degree since 2021. He earned his B.Sc. and M.Sc. degrees from National Taiwan University (NTU) in 2013 and 2015, respectively. From 2016 to 2021, he worked as a machine learning researcher at several international AI startups. He is currently a member of the Multiscale Networked Systems (MNS) Group. His recent research centers on leveraging AI and machine learning for network resource management.



**Jorge Martín Pérez** is an associate professor at the Universidad Politécnica de Madrid (UPM), Spain. He obtained a B.Sc in mathematics, and a B.Sc in computer science, both at Universidad Autónoma de Madrid (UAM) in 2016. He obtained his M.Sc. and Ph.D in Telematics from Universidad Carlos III de Madrid (UC3M) in 2017 and 2021, respectively. Jorge worked as postdoc at UC3M (until 2023) in national and EU funded projects. His research focuses in optimal resource allocation in networks.



**Danny De Vleschauer** obtained an MSc. in Electrical Engineering and the Ph.D. degree in applied sciences from the Ghent University, Belgium, in 1985 and 1993 respectively. Currently, he is a DMTS in the access network control department of Nokia Bell Labs in Antwerp, Belgium. He was a researcher at Ghent University before joining Nokia. His early work was on image processing and on the application of queuing theory in packet-based networks. His current research focus is on the distributed control of applications over packet-based networks.



Luca Valcarengi is an associate professor at the Scuola Superiore Sant'Anna of Pisa, Italy, since 2014. He published almost three hundred papers (source Google Scholar, May 2020) in International Journals and Conference Proceedings. He received a Fulbright Research Scholar Fellowship in 2009 and a JSPS "Invitation Fellowship Program for Research in Japan (Long Term)" in 2013. His main research interests are optical networks design, analysis and optimization; communication networks reliability; energy efficiency in communications networks; optical access networks; zero touch network and service management; experiential networked intelligence; 5G technologies and beyond.



Xi Li received her M.Sc in electronics and telecommunication engineering from Technische Universität Dresden in 2002 and her Ph.D. from the University of Bremen in 2009. Between 2003 and 2014 she worked as a research fellow and lecturer at the Communication Networks Group in the University of Bremen, leading a team working on several industrial and European R&D projects on 3G/4G mobile networks and future Internet design. From 2014 to 2015 she worked as a solution designer in Tele-fonica Germany GmbH & Co. OHG, Hamburg. Since March 2015 she has been a senior researcher in 5G Networks R&D at NEC Laboratories Europe.



Chrysa Papagianni is an associate professor at the Informatics Institute of the University of Amsterdam. She is part of the Multiscale Networked Systems group that focuses its research on network programmability and data-centric automation. Her research interests lie primarily in the area of programmable networks with emphasis on network optimization and the use of machine learning in networking. She has worked in multiple research projects funded by the European Commission, the Dutch research council and the European Space Agency, such as 5Growth, CATRIN, etc. Chrysa is currently coordinating the SNS JU DESIRE6G project on 6G system architecture. She also leads the AI-assisted networking work package in the 6G flagship project for the Netherlands on Future Network Services.